Published online 5 January 2011 *Nucleic Acids Research, 2011, Vol. 39, No. 8* ***3427–3445***
doi:10.1093/nar/gkq1328

Determinants of Nam8-dependent splicing of meiotic pre-mRNAs

Zhicheng R. Qiu[1], Beate Schwer[2,*] and Stewart Shuman[1,*]

[1]Molecular Biology Program, Sloan-Kettering Institute and [2]Department of Microbiology and Immunology, Weill Cornell Medical College, New York, NY 10065, USA

Received November 16, 2010; Revised December 13, 2010; Accepted December 14, 2010

ABSTRACT

Nam8, a component of yeast U1 snRNP, is optional for mitotic growth but required during meiosis, because Nam8 collaborates with Mer1 to promote splicing of essential meiotic mRNAs *AMA1, MER2 and MER3*. Here, we identify *SPO22* and *PCH2* as novel targets of Nam8-dependent meiotic splicing. Whereas *SPO22* splicing is co-dependent on Mer1, *PCH2* is not. The *SPO22* intron has a non-consensus 5′ splice site (5′SS) that dictates its Nam8/Mer1-dependence. *SPO22* splicing relies on Mer1 recognition, via its KH domain, of an intronic enhancer 5′-AYACCCUY. Mutagenesis of KH and the enhancer highlights Arg214 and Gln243 and the CCC triplet as essential for Mer1 activity. The Nam8-dependent *PCH2* pre-mRNA has a consensus 5′SS and lacks a Mer1 enhancer. For *PCH2*, a long 5′ exon and a non-consensus intron branchpoint dictate Nam8-dependence. Our results implicate Nam8 in two distinct meiotic splicing regulons. Nam8 is composed of three RRM domains, flanked by N-terminal leader and C-terminal tail segments. The leader, tail and RRM1 are dispensable for splicing meiotic targets and unnecessary for vegetative Nam8 function in multiple synthetic lethal genetic backgrounds. Nam8 activity is enfeebled by alanine mutations in the putative RNA binding sites of the RRM2 and RRM3 domains.

INTRODUCTION

Regulated pre-mRNA splicing figures prominently in the control of eukaryal gene expression. Alternative splice site utilization amplifies the information content of the human genome (1,2), allowing a single transcription unit to generate multiple protein products that may differ in their domain composition, cellular localization, macromolecular interactions or biochemical activities. Splicing control receives numerous inputs in metazoan organisms: (i) from *cis*-acting RNA sequences or secondary structures that modulate interactions of the splicing machinery with pre-mRNA (3) and (ii) from a fleet of RNA-binding proteins (4) that enhance or silence splicing in response to these RNA signals, to changes in the cellular milieu, and to developmental cues (2,5,6). Defects or imbalances in pre-mRNA splicing underlie a broad spectrum of human diseases, either via mutations of core splicing machinery and splicing regulatory factors or, more commonly, mutations of RNA signals that direct or regulate splice site utilization (7).

Yeast has been a powerful model system to elucidate the composition and function of the core splicing machinery (8) and the dynamic changes in the spliceosome that propel splicing chemistry and fidelity (9). Although budding yeast has relatively few natural examples of splicing regulation via alternative 5′ splice site choice, alternative 3′ splice site choice or exon skipping (10–12), it relies heavily in meiosis on controlling the mode of alternative splicing known as intron retention (2). To wit, the meiotic developmental program entails a shift in the processing patterns of target pre-mRNAs from a vegetative 'off' state, in which single introns are included, to a meiotic 'on' state in which the target introns are removed. The discovery of Mer1-regulated meiotic splicing and the appreciation that Mer1 functions together with Nam8 to compensate for inherently weak introns are landmarks in the field (13–15).

Nam8 is an RNA-binding component of the yeast U1 snRNP and is present in the commitment complex of U1 snRNP at the 5′ splice site, where it can be crosslinked to the pre-mRNA (16–18). The Nam8 protein contains three tandem RRM domains and is a putative yeast homolog of the mammalian RNA-binding protein and pre-mRNA splicing factor TIA-1 (19,20). Nam8 is inessential for yeast mitotic growth, but is essential for yeast sporulation because it promotes splicing of a small set of specific mRNAs that encode proteins required for meiotic

*To whom correspondence should be addressed. Tel: +1 212 639 7145; Fax: +1 212 717 3623; Email: s-shuman@ski.mskcc.org
Correspondence may also be addressed to Beate Schwer. Tel: +1 212 746 6518; Fax: +1 212 746 8587; Email: bschwer@med.cornell.edu

recombination and cell division (15,21–23). Nam8-dependent splicing of three meiotic mRNAs – *AMA1*, *MER2* and *MER3* – is activated by the meiotic splicing regulator Mer1 (13,24). Mer1 is produced only in meiotic cells under the control of the meiotic transcription factor Ime1 (25). Mer1 activates splicing by binding to an intronic splicing enhancer sequence (5′-AYACCCUY-3′) present in the *AMA1*, *MER2* and *MER3* pre-mRNAs (15). Mer1 bound to the intronic enhancer is thought to promote assembly of the U1 and U2 snRNPs on the pre-mRNA (22,26). Transcripts subject to Mer1/Nam8 splicing regulation have suboptimal 5′ splice sites and, in some cases, suboptimal branchpoints or a large 5′ exon that might, alone or together, dictate their reliance on otherwise inessential splicing factors (14,22,27).

Recent studies have illuminated additional meiotic intron-containing genes as potential targets of regulated splicing, several of which do not contain a Mer1 enhancer (10,28–31). Here, by evaluating the splicing of the known meiotic intron-containing RNAs in wild-type and *nam8Δ* yeast diploids during attempted sporulation, we discovered that Nam8 has two additional meiotic mRNAs targets: *SPO22* and *PCH2*. The *SPO22* intron contains a Mer1 binding site and requires both Nam8 and Mer1 for splicing. By contrast, *PCH2* lacks a Mer1 site and is indifferent to the presence of Mer1 for its splicing. We interrogated the prevailing hypothesis that meiotic splicing controllers such as Mer1 and Nam8 compensate for weak intronic splicing signals and/or override negative influences exerted by other RNA elements. We elucidated these RNA features for *SPO22*, *MER3* and *PCH2*. A structure-guided mutational analysis of the putative RNA binding site of Mer1 identified individual amino acid functional groups required for its splicing enhancement activity *in vivo*. Mutational analysis of Nam8 demarcated domain requirements for meiotic splicing and for Nam8 function in vegetative cells that require Nam8 for growth because they lack other inessential splicing factors.

METHODS

Yeast strains for sporulation studies

The meiosis/sporulation experiments were carried out with isogenic diploids in the SK1 background. To generate the *nam8Δ* diploids, haploid derivatives of the SK1 strain, SKY163 (*MAT*a *ho::LYS2 lys2 ura3 leu3::hisG*) and SKY164 (*MATα ho::LYS2 lys2 ura3 leu3::hisG*) were used. In brief, a DNA segment encompassing the *nam8::kanMX* disruption cassette was generated by polymerase chain reaction (PCR) amplification of genomic DNA from a *nam8::kanMX* yeast strain, the PCR product was introduced into SKY163, and geneticin-resistant *kanMX* integrants were selected. SKY164 was transformed with a *nam8::natMX* deletion cassette (32,33) and nourseothricin-resistant *natMX* integrants were selected. The targeted insertions were confirmed by diagnostic Southern blotting. The SKY haploids were then mated and homozygous *nam8Δ* diploids were selected on YPD agar containing 100 μg/ml nourseothricin (clonNat, Werner BioAgents, Jena) and 150 μg/ml geneticin (Invitrogen).

Sporulation and analysis of meiotic RNA splicing

Single colonies of wild-type and *nam8Δ* diploid yeast strains were patched on agar plates with glycerol as the carbon source for at least 6 h to select for cells with healthy mitochondria. Cells were streaked on YPD agar plates and incubated for 3 days at 30°C. Single colonies were then inoculated into YPD liquid medium and grown at 30°C to stationary phase (A_{600} of 6–8). Aliquots were inoculated into 12.5 ml of presporulation medium (0.5% yeast extract, 1% peptone, 0.67% yeast nitrogen base (without amino acids), 1% potassium acetate, 0.05 M potassium biphthalate (pH 5.5), 0.002% antifoam 204) to attain an A_{600} of 0.8. The cultures were incubated for 7 h at 30°C and added to 100 ml of fresh presporulation medium to attain an A_{600} of 0.025. After 16 h incubation at 30°C, the cells were washed twice with 100 ml of sporulation medium (2% potassium acetate, 0.001% polypropylene glycol) and resuspended in 15 ml of sporulation medium to attain an A_{600} of 6. For analysis of meiotic RNA, 2-ml aliquots of the cultures were withdrawn immediately prior to transfer to sporulation medium and at 4 h and 8 h post-transfer to sporulation medium. Cells were harvested by centrifugation and RNA was extracted from the cells by using the MasterPure Yeast RNA Purification Kit (Epicentre BioTechnologies). The DNase digestion step in the RNA purification protocol was modified such that the samples were incubated for 1 h with 20 U of RNase-free DNase I (New England Biolabs) to eliminate genomic DNA. First-strand cDNA was synthesized in reaction mixtures containing 10 ng/μl total RNA, 25 ng/μl oligo(dT)$_{12–18}$ primer, 10 U/μl SuperScript II (Invitrogen), 1 X First Strand Buffer, 10 mM DTT and 0.5 mM dNTPs. RNA, dNTPs and primers were preincubated for 5 min at 65°C before quick chilling on ice. DTT and First Strand Buffer were added, and the mixture was incubated at 42°C for 2 min. Finally, reverse transcriptase was added and the reaction mixture was incubated at 42°C for 50 min and then at 70°C for 15 min. The cDNAs for meiotic transcripts were then PCR-amplified in 25 μl reaction mixtures containing 1X native *Pfu* buffer, 0.2 mM dNTPs, 0.8 μM gene-specific sense strand primer and 0.8 μM 5′-^{32}P-labeled gene-specific antisense strand primer (Supplementary Table S1), 0.05 U/μl *Pfu* DNA Polymerase (Agilent Technologies) and 2 μl of each cDNA sample. The PCR cycles (n = 31) entailed incubations at 94°C for 30 s, 55°C for 90 s, and 72°C for 2 min. The RT–PCR products were analyzed by electrophoresis through 2% native agarose gels. After electrophoresis, the gels were stained with ethidium bromide and then dried under vacuum on DEAE paper. The ^{32}P-labeled PCR products were visualized by autoradiography and quantified by scanning with a Fuji BAS-2500 imager.

Assay of splicing of meiotic RNAs in vegetative cells

A haploid 'wild-type' *NAM8* yeast strain (*MAT*a *NAM8 leu2Δ ura3Δ*), derived from S288c, and a *nam8::kanMX*

and variants thereof (32) were transformed with plasmid pYX212-MER1 (2 μ *URA3 MER1*) expressing the *MER1* open reading frame under the transcriptional control of the yeast *TPI1* promoter (see below), or with the empty pYX212 vector. Cells were cotransformed with 2 μ plasmids bearing *SPO22*, *MER3* or *PCH2* genes as specified in the figure legends. pRS425TPI-SPO22 (2 μ *LEU2 SPO22*) carries the intron-containing *SPO22* gene driven by the *TPI1* promoter. pRS425TPI-MER3 (2 μ *LEU2 MER3*) carries the intron-containing *MER3* gene driven by the *TPI1* promoter. pRS425-PCH2 (2 μ *LEU2 PCH2*) bears the intron-containing *PCH2* gene (from 540 bp upstream of the translation start codon to 265 bp downstream of the stop codon) under the control of its native promoter. Intron mutants were generated by two-stage overlap extension PCR with mutagenic primers; the mutated DNAs were inserted into pRS425. The inserts of all plasmid clones were sequenced to exclude the acquisition of unwanted mutations during amplification and cloning.

The haploid plasmid-bearing yeast strains were grown in SD-(Ura$^-$Leu$^-$) liquid medium at 30°C until A_{600} reached 2–4. Cells were harvested by centrifugation from 2-ml aliquots of the cultures. RNA extractions and reverse transcription–polymerase chain reaction (RT–PCR) were performed as described above, with exceptions as follows: (i) cDNA synthesis was primed with 0.1 μM gene-specific antisense primers (Supplementary Table S1) instead of oligo(dT)$_{12–18}$; (ii) the numbers of PCR cycles for amplification of *MER2, PCH2, SPO22* and *MER3* cDNAs were 28, 27, 25 and 23, respectively; (iii) the PCR reactions were quenched by adding EDTA and SDS to a final concentrations of 12.5 mM and 3.3%, respectively; and (iv) the ^{32}P-labeled PCR products were analyzed by electrophoresis through native 5% polyacrylamide gels containing 90 mM Tris-borate, 1.2 mM EDTA.

Mer1 mutants

The *MER1* open reading frame was amplified by PCR from yeast genomic DNA using primers designed to introduce an EcoRI site immediately upstream of the translation initiation codon and an XhoI site immediately downstream of the stop codon. The PCR product was inserted into yeast expression vector pYX212 (2 μ *URA3*) to yield pYX212-MER1. Truncated *MER1-NΔ* alleles were constructed by PCR amplification of pYX212-MER1 template with sense-strand primers that introduced a new start codon at the positions specified plus a flanking EcoRI site. Missense mutations were introduced into the *MER1* ORF via a two-stage overlap extension PCR. The PCR products of the truncated and mutated *MER1* ORFs were digested with EcoRI and XhoI and inserted into EcoRI/XhoI-cut pYX212-MER1 in lieu of the wild-type gene.

Yeast Nam8 expression vectors

To construct the *NAM8* vectors for plasmid shuffle complementation assays, a 1.6-bp DNA fragment comprising the *NAM8* ORF plus 427 bp of upstream (5′) and 277 bp of downstream (3′) chromosomal DNA was amplified by PCR from *Saccharomyces cerevisiae* genomic DNA using primers that introduced a HindIII site at the 5′ end and a SacI site at the 3′ end. We then used overlap extension PCR to introduce a PstI site immediately upstream of the *NAM8* translation initiation codon and an XbaI site immediately downstream of the stop codon. The *NAM8* cassette (ORF plus flanking DNA) was then inserted into yeast expression vector pRS415 (*CEN LEU2*) to yield pRS415-NAM8. The truncated *NAM8* alleles were constructed by PCR amplification with: (i) sense strand primers that introduced a new start codon at the positions specified plus a flanking PstI site and (ii) antisense strand primers that introduced a new stop codon after the positions specified plus a flanking XbaI site. Missense mutations were introduced into the *NAM8* ORF via two-stage overlap extension PCR. The PCR products containing the truncated and mutated *NAM8* ORFs were digested with PstI and XbaI and inserted into PstI/XbaI-cut pRS415-NAM8 in lieu of the wild-type gene.

To construct vectors for *NAM8* overexpression, the *NAM8* ORFs encoding wild-type, truncated or mutated Nam8 were amplified by PCR from their respective pRS415 plasmids using sense primers that introduced a KpnI site immediately flanking the start codon. The PCR products were digested with KpnI/XbaI and inserted into KpnI/XbaI-cut pYES2 (2 μ *URA3 GAL*) so as to place *NAM8* under the transcriptional control of a glucose-repressible/galactose-inducible *GAL1* promoter.

All of the *NAM8* plasmid inserts were sequenced completely to exclude the acquisition of unwanted mutations during amplification and cloning.

Yeast strains for assays of Nam8 function in vegetative cells

Saccharomyces cerevisiae strain yTN (*Mata tgs1Δ nam8Δ* p360-TGS1), described in Hausmann *et al.* (32) was used for plasmid shuffle complementation assays of Nam8 function. We constructed other *nam8Δ* double mutant strains by crossing and dissecting haploid strains that were described previously (32,33). In brief, haploid *nam8::natR* cells were mixed with *lea1::kanMX*, *mud1::kanMX* and *mud2::kanMX* cells of the opposite mating type, and diploids were selected on YPD agar containing nourseothricin and geneticin. The heterozygous diploids were transformed with a *URA3 CEN* plasmid carrying the *NAM8* gene. Sporulation was induced and tetrads were dissected. Individual spores were tested to select for *nam8Δ::natR mud1Δ::kanMX* p360-NAM8, *nam8Δ::natR mud2Δ::kanMX* p360-NAM8 or *nam8Δ::natR lea1Δ::kanMX* p360-NAM8 cells. Using the same strategy, we also generated *nam8Δ::natR mud2Δ::kanMX* p360-MUD2, in which the complementing *URA3* plasmid harbors the *MUD2* gene (33).

HIS3 reporter assay for *PCH2* intron splicing

To generate integration cassettes for the *HIS3* reporter genes, a 1-bp genomic DNA fragment spanning the *HIS3* ORF plus 297 and 20 bp of upstream and downstream sequences was amplified by PCR using primers His3-F and His3-R (Supplementary Table S2) and

inserted in between the XmaI and PstI sites in pUC19. To insert the *PCH2* intron (or the mutated *PCH2-BP* intron) at position 430 in the *HIS3* ORF, we individually amplified the *HIS3-5′* gene fragment (727 bp) with primers His3-F and exon1R (Supplementary Table S2) and the *HIS3-3′* (253 bp) gene fragment with His3-R and exon2F (Table S2). The *PCH2* and *PCH2-BP* introns (123 bp) were amplified by PCR with primers IntronF and IntronR. The exon and intron DNA fragments with overlapping terminal sequences were then assembled into intron-punctuated *HIS3* cassettes by overlap-extension PCR and the cassettes were inserted into pUC19 plasmids. The *HIS3*, *HIS3-[PCH2]* and *HIS3-[PCH2-BP]* cassettes were excised with SmaI and PstI and transformed into *nam8Δ::natR* p360-NAM8 (*URA3 NAM8*) cells and isogenic wild-type cells (harboring a *URA3* plasmid) that were histidine-auxotrophs. His^+Ura^+ transformants were selected and analyzed for integration of the respective cassettes at the *HIS3* locus by diagnostic Southern blotting and by sequencing of PCR-generated DNA fragments using primers designed to amplify the *HIS3* gene. The cells were then streaked to medium containing 5-FOA (and histidine) to select for cells that had lost the *URA3* plasmids. Individual colonies were patched to YPD agar. Cells were grown in liquid YPD medium until the cultures attained A_{600} between 0.7 and 0.9. The cultures were diluted in water to A_{600} of 0.01. Serial 10-fold dilutions were prepared and aliquots (3 µl) of each were spotted in parallel on YPD agar and SD agar medium lacking histidine.

RESULTS

Meiotic splicing in *nam8Δ* cells

RNA was isolated from wild-type and *nam8Δ* diploids immediately prior to (time 0) and 4 h and 8 h after transfer from pre-sporulation medium to sporulation medium. cDNA was prepared from each RNA sample by RT and then used for gene-specific PCR amplification of meiotic spliced transcripts (Figure 1 and Table 1). The sense and antisense primers corresponded to sequences flanking the introns so that the longer products of amplification of cDNA derived from unspliced pre-mRNAs could be easily resolved by native gel electrophoresis from the shorter products of amplification of cDNAs copied from spliced mRNA (Figure 1). One of the primers was 5′ ^{32}P-labeled in each PCR reaction so that we could quantify the distributions of unspliced and spliced cDNAs for each gene of interest (Figure 1, lanes 3–5). An aliquot of a PCR amplification reaction using genomic DNA as template provided a marker for the unspliced species (lane 2). No labeled products were generated from PCR reactions programmed by RNA that had not been subjected to prior treatment with reverse transcriptase (lane 1), indicating that the RNA samples were effectively free of contaminating genomic DNA.

Figure 1 shows exemplary data demonstrating induction of meiotic transcription and regulated meiotic splicing in wild-type cells, while focusing on some of the meiotic transcripts for which splicing efficiency was most acutely affected by the absence of Nam8. Transcriptional induction of the *MER3* gene in wild-type cells was evinced by the increase in total RT–PCR products at 4 and 8 h post-sporulation (lanes 4 and 5) compared to the level at time 0 (lane 3), which was accompanied by a sharp increase in the percentage of the RT–PCR product derived from spliced versus unspliced *MER3* RNA. In agreement with previous studies (34,35), we also observed transcriptional induction of *SPO22* and *PCH2* (Figure 1) and of several other intron-containing meiotic genes analyzed (data not shown). Transcriptional induction of *MER3*, *SPO22*, *PCH2* and other meiotic genes was also evident in *nam8Δ* cells after 4 and 8 h in sporulation medium (Figure 1 and data not shown).

The role of Nam8 in meiotic splicing was verified for *MER3* (one of three known Mer1/Nam8 targets), splicing of which was barely detectable in *nam8Δ* cells at either 4 or 8 h (Figure 1). Nam8 was also required for meiotic splicing of *SPO22* and *PCH2* pre-mRNAs (Figure 1), which are hereby identified as new Nam8 targets. By contrast, the control *GLC7* RNA was constitutively expressed and very efficiently spliced in wild-type cells (≥98% of the RT–PCR product was from spliced *GLC7* RNA) and this was unaffected by *nam8Δ* (Figure 1).

The results of our survey of splicing of 14 meiotic transcripts at 4 h post-induction of sporulation are compiled in Table 1, wherein each datum for splicing efficiency – [spliced/(spliced + unspliced)] × 100 – is the average of three independent sporulation experiments and RT–PCR analyses. The absence of Nam8 severely affected meiotic splicing of *AMA1*, *MER2* and *MER3* (the three Nam8 targets described previously) plus novel targets *SPO22* and *PCH2*. Nam8 ablation had little or no impact on the efficiency of splicing of the *HOP2*, *REC114*, *MEI4*, *REC102*, *DMC1*, *SPO1*, *MND1* and *SRC1* transcripts (Table 1), though *nam8Δ* did reduce *SAE3* splicing modestly.

Inspection of the features of the 14 meiotically spliced transcripts reveals that four of them—*AMA1*, *MER2*, *MER3* and *SPO22*—have a Mer1 intronic enhancer, thereby extending the correlation of coregulation by Mer1 and Nam8 to the *SPO22* pre-mRNA identified presently as Nam8 dependent. The magnitudes of the *nam8Δ* splicing defects for the four Mer1 enhancer-containing transcripts were between 12- and 40-fold (Table 1). To our knowledge, *PCH2* is the first instance of a Nam8-dependent meiotic pre-mRNA that does not have a Mer1 intronic consensus sequence. The decrement in *PCH2* splicing in the *nam8Δ* strain was 8-fold.

Differential requirements for Mer1 in splicing of *SPO22* and *PCH2* mRNAs

Regulated splicing of Mer1-dependent meiotic mRNAs can be recapitulated in vegetative yeast cells by forced expression of the Mer1 splicing enhancer protein (13,15.23). The efficacy of this maneuver is readily demonstrated for splicing of the *MER2* pre-mRNA, which is constitutively transcribed in vegetative cells, but is spliced inefficiently (20%) because Mer1 is absent (Figure 2A). Expression of Mer1 during vegetative

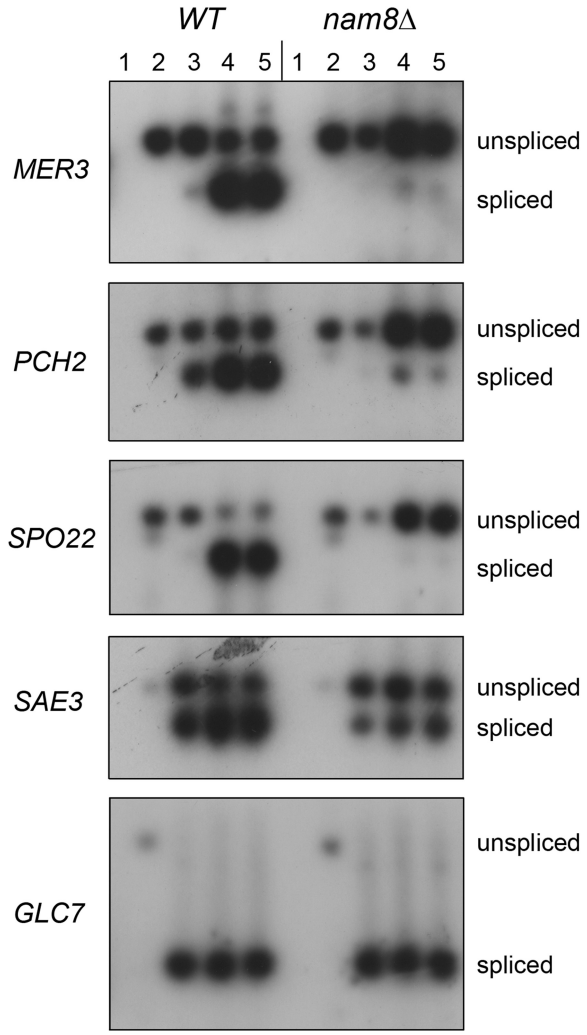

Figure 1. Meiotic splicing in wild-type and *nam8*Δ yeast cells. RNAs isolated from wild-type and *nam8Δ* diploid strains sampled immediately prior to transfer to sporulation medium (lane 3) or 4 h (lane 4) and 8 h (lane 5) post-transfer to sporulation medium were reverse transcribed and the cDNAs were PCR-amplified with gene-specific primers flanking the introns of meiotic transcripts *MER3, PCH2, SPO22* and *SAE3* and the constitutively spliced *GLC7* transcript. The antisense PCR primers were 5′ ^{32}P-labeled in each case. The labeled PCR products were resolved by native agarose gel electrophoresis and visualized by autoradiography. The RNA samples in lane 1 were PCR-amplified without reverse transcription, as a control for potential genomic DNA contamination. Lane 2 includes aliquots of the products of PCR-amplification of genomic DNA, which are the same sizes as the RT–PCR products derived from the intron-containing RNAs. The positions of the RT–PCR products of unspliced and spliced transcripts are indicated at 'right'.

growth (by transformation with a plasmid bearing *MER1* under the control of a constitutive promoter) increased *MER2* splicing efficiency to 87% (Figure 2A). *MER2* splicing was inhibited severely (5% efficiency) in *nam8*Δ cells expressing Mer1 (Figure 2A).

To test whether *SPO22* or *PCH2* pre-mRNA splicing relies on Mer1, we transformed vegetative cells with 2 μ plasmids bearing *SPO22* or *PCH2* genes plus a second plasmid for constitutive *MER1* expression (or an empty vector control). Splicing of *SPO22* mRNA was acutely

Table 1. Meiotic mRNA splicing efficiency: effects of *nam8*

RNA	Percent spliced at 4 h	
	WT	*nam8Δ*
AMA1	84 ± 5	6 ± 3
MER2 (REC107)	76 ± 2	6 ± 3
MER3 (HFM1)	80 ± 2	2 ± 1
HOP2	88 ± 6	84 ± 4
REC114	87 ± 1	76 ± 2
MEI4	80 ± 1	71 ± 2
REC102	84 ± 4	74 ± 4
DMC1	95 ± 1	95 ± 3
PCH2	73 ± 2	9 ± 2
SAE3	66 ± 1	37 ± 2
SPO1	84 ± 3	80 ± 4
SPO22	86 ± 1	4 ± 2
MND1	90 ± 4	82 ± 3
SRC1	94 ± 2	87 ± 2

dependent on Mer1 (86% in Mer1-expressing cells versus 14% in control cells) and Nam8 (4% splicing in Mer1-expressing *nam8*Δ cells) (Figure 2B). By contrast, splicing of *PCH2* (at 67% efficiency in wild-type vegetative cells, comparable to that seen in meiotic cells; Table 1) was unaffected by Mer1 expression (Figure 2C). These results consolidate the following points: (i) *SPO22*, which contains an intronic Mer1 enhancer element, joins three other meiotic genes—*AMA1*, *MER2* and *MER3*—to comprise a splicing regulon controlled by *both* Mer1 and Nam8; (ii) *PCH2* is the first instance of a Mer1-independent Nam8-regulated meiotic transcript.

Why does *SPO22* splicing depend on Mer1 and Nam8?

SPO22 has a consensus Mer1 enhancer element (5′-AUAC CCUU) situated between the 5′ splice site and the branchpoint (Figure 3A). *SPO22* is especially interesting, *vis à vis* other Mer1 targets, in that its intron has multiple features that could confer feeble splicing and hence reliance on upregulation. These include: (i) a rare non-consensus 5′ splice site (GUAUAU) distinct from those in other Mer1-dependent transcripts; (ii) a rare non-consensus branchpoint (AACUAAC); and (iii) a non-consensus 3′ splice site (AAG) (Figure 3A). Analysis of the *SPO22* intron in Mfold (36) revealed no stable secondary structure that would mask any of these signals.

We installed consensus *5′SS*, *BP* and *3′SS* elements in the *SPO22* gene and tested these *SPO22* mutants on 2 μ plasmids for their splicing efficiency in vegetative wild-type and *nam8*Δ cells that do or do not express Mer1. Our aim here was to pinpoint which of the intron manipulations might render *SPO22* splicing independent of Mer1 and/or Nam8. In particular, we wished to see if the degrees of Nam8 and Mer1 dependence tracked together, or if we could find an intronic manipulation that dissociated Mer1 from Nam8 (e.g. relieving the requirement for one factor, but not the other). The *SPO22* splicing efficiencies are plotted in Figure 3A, with each datum representing the average of three separate experiments ± SEM.

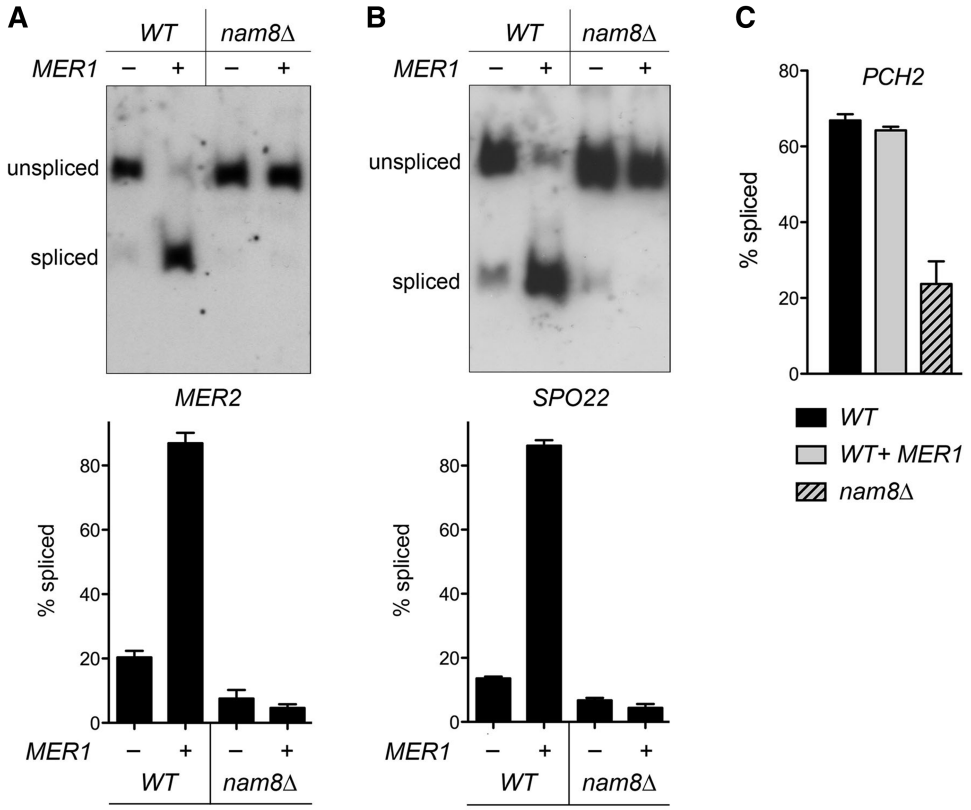

Figure 2. Nam8 and Mer1 requirements for splicing of meiotic *SPO22* and *PCH2* mRNAs can be gauged in vegetative cells. Endogenous *MER2* transcripts (**A**) and transcripts derived from plasmid-borne meiotic genes *SPO22* (**B**) and *PCH2* (**C**) were analyzed by RT–PCR with gene-specific primers using total RNA template isolated from wild-type or *nam8Δ* haploids that carried either a 2 μ plasmid for constitutive expression of Mer1 (*MER1*$^{+}$) or an empty 2 μ plasmid control (*MER1*$^{-}$). The antisense PCR primers were 5′ ^{32}P-labeled in each case. The PCR products were analyzed by 5% native PAGE and visualized by autoradiography of the dried gels (A and B, top panels). The RT–PCR products derived from unspliced and spliced transcripts were quantified and the splicing efficiencies (percentage spliced = spliced /(spliced + unspliced) × 100) are plotted (A and B, bottom panels; C). Each datum is the average of three separate experiments ± SEM.

We found that installing a perfect GUAUGU 5′ splice site (via a single A-to-G change in mutant *SPO22-5′SS*) eliminated the dependence of *SPO22* splicing on Mer1, i.e. basal splicing efficiency was increased to 92% in wild-type yeast lacking Mer1 and this value was unaffected by Mer1 expression (Figure 3A). Similarly, the consensus *5′SS* change effaced the dependence of *SPO22* splicing on Nam8, elevating splicing efficiency to 86% in *nam8Δ* cells lacking Mer1 (Figure 3A). We surmise that the nonconsensus 5′ splice site is the critical determinant of the Mer1/Nam8 requirement for efficient *SPO22* splicing *in vivo*.

By contrast, whereas the installation of a consensus branchpoint (entailing a A-to-U mutation in *SPO22-BP*) or a consensus 3′ splice site (UAG in *SPO22-3′SS*) raised basal splicing efficiency in wild-type cells to 51% and 28%, respectively (versus 14% for native *SPO22*), the *SPO22-BP* and *SPO22-3′SS* transcripts remained dependent on Mer1 to attain their optimal splicing efficiencies of 86% and 90%, respectively (Figure 3A). The increases in basal splicing in *nam8Δ* cells for the *SPO22-BP* and *SPO22-3′SS* mutants (to 28% and 16%, respectively, versus 6% for the native *SPO22* transcript) were of lesser magnitude than that seen in *NAM8* cells. Moreover, there was no further increase in splicing of the *SPO22-BP* and *SPO22-3′SS* mutants in *nam8Δ* cells attendant on Mer1 expression (Figure 3A). These results indicate that: (i) all of the salutary effects of Mer1 on *SPO22* splicing are mediated via Nam8, but not *vice versa*; (ii) even in the absence of Mer1, Nam8 has a modest positive effect (~2-fold stimulation) on basal *SPO22* splicing, be it in the context of the feebly spliced native *SPO22* intron or the better-spliced consensus *BP* and *3′SS* variants; and (iii) the non-consensus branchpoint and 3′ splice site of *SPO22* each exerts a suppressive effect on intron removal that is 'independent' of Nam8, with the non-consensus branchpoint effect being of greater magnitude.

Determinants of *MER3* pre-mRNA splicing

Inspection of the *MER3* intron, which requires Mer1 and Nam8 for splicing in meiosis (35), reveals several features not found in other Mer1/Nam8 targets. These include: (i) a deviant 5′SS (GUAGUA) found in no other yeast introns (37,38); (ii) a rare non-consensus branchpoint (GACUAAC); (iii) an exceptionally long distance (83-nt) from the BP to the 3′SS (38); and (iv) a 12-nt polypyrimidine tract (5′-CCUCUUUCUUUU) between the BP and 3′SS, placed close to the branchpoint

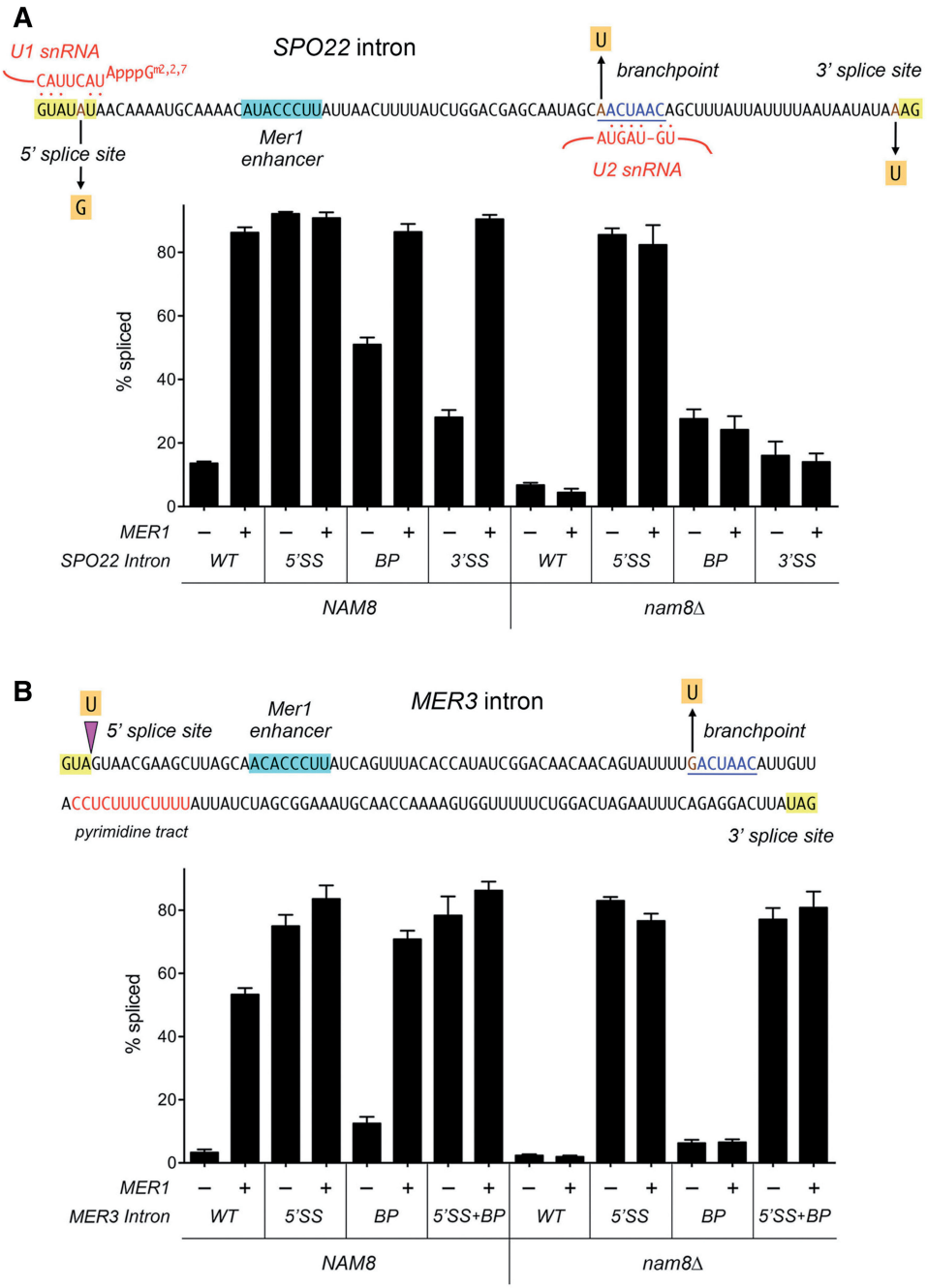

Figure 3. Intronic determinants of the Nam8 and Mer1 dependence of *SPO22* and *MER3* pre-mRNA splicing. (**A**) The nucleotide sequence of the *SPO22* intron is shown, highlighting its nonconsensus 5′ splice site, branchpoint and 3′ splice site, and the location of its putative Mer1 enhancer. Base pairing interactions with U1 snRNA at the 5′ splice site and with U2 snRNA at the branchpoint are shown. The point mutations (*5′SS*, *BP* and *3′SS*) that we introduced into the *SPO22* intron are indicated. Splicing was gauged by RT–PCR with *SPO22*-specific primers using total RNA template isolated from wild-type (*NAM8*) or *nam8Δ* haploids that had been transformed with 2 μ *SPO22* or its intron mutant variants as specified plus a 2 μ plasmid for constitutive expression of Mer1 (*MER1*$^{+}$) or an empty 2 μ plasmid control (*MER1*$^{-}$). The antisense PCR primers were 5′ ^{32}P-labeled in each case. The RT–PCR products derived from unspliced and spliced transcripts were resolved by native 5% PAGE and quantified. The splicing efficiencies are plotted for the *NAM8* and *nam8*Δ strains. Each datum is the average of three separate experiments ± SEM. (**B**) The nucleotide sequence of the *MER3* intron is shown, highlighting its nonconsensus 5′ splice site and branchpoint, and the location of its putative Mer1 enhancer. The point mutations (*5′SS* and *BP*) that we introduced into the *MER3* intron are indicated. Splicing was gauged by RT–PCR with *MER3*-specific primers using total RNA template isolated from wild-type (*NAM8*) or *nam8Δ* haploids that had been transformed with 2 μ *MER3* or its intron mutant variants as specified plus a 2 μ plasmid for constitutive expression of Mer1 (*MER1*$^{+}$) or an empty 2 μ plasmid control (*MER1*$^{-}$). The splicing efficiencies are plotted for the *NAM8* and *nam8*Δ strains. Each datum is the average of three separate experiments ± SEM.

(Figure 3B). Unlike *SPO22*, *MER3* has a typical UAG 3′ splice site that is utilized to generate the correctly spliced *MER3* mRNA that encodes the 1187-aa Mer3 polypeptide (Figure 3B). *MER3* also has three other YAG triplets (potential 3′ splice sites) located between the branchpoint/polypyrimidine tract and the correct 3′SS (Figure 3B); utilization of any of these alternative 3′SS would generate out-of-frame transcripts with premature stop codons.

We initiated an analysis of *MER3* splicing requirements by installing consensus *5′SS* and *BP* signals in the *MER3* gene, singly and in combination. Native and mutated *MER3* alleles on 2 μ plasmids were then assayed by RT–PCR for their splicing efficiency in vegetative wild-type and *nam8*Δ cells that do or do not express Mer1. Splicing of native *MER3* mRNA was dependent on Mer1 (53% in Mer1-expressing cells versus 3% in control cells) and Nam8 (2% splicing in Mer1-expressing *nam8*Δ cells) (Figure 3B). Introducing a perfect GUAUGU 5′ splice site (via a single U insertion in mutant *MER3-5′SS*) increased basal splicing efficiency to 75% in wild-type yeast lacking Mer1, and enhanced the extent of splicing in the presence of Mer1 to 84% (Figure 3B). By contrast, the consensus *BP* change *per se* elicited a relatively modest elevation in basal *MER3* splicing (to 12%) while the *MER3-BP* intron remained Mer1-dependent, with splicing efficiency rising to 71% in wild-type cells expressing Mer1 (Figure 3B). The effects of combining the *MER3 5′SS* and *BP* changes (resulting in 78% and 86% splicing in the absence and presence of Mer1, respectively) were virtually identical to those seen for the single *5′SS* change (Figure 3B). These results signify that the aberrant *MER3* 5′ splice site is the principal determinant of the Mer1 requirement for splicing *in vivo*.

The *5′SS* change eliminated the dependence of *MER3* splicing on Nam8, elevating splicing efficiency to 83% in *nam8*Δ cells lacking Mer1 (Figure 3B). The consensus *BP* change conferred no such benefit *per se* (6% splicing with or without Mer1) and had no additive effects in *nam8Δ* cells when combined with the consensus 5′SS mutation (Figure 3B). We surmise that the weak 5′ splice site is the critical determinant of the Nam8 requirement for efficient *MER3* splicing.

Requirements for Mer1 enhancer elements in the *MER3* and *SPO22* introns

Spingola and Ares (15) identified a *cis*-acting intronic splicing enhancer, of consensus sequence 5′-AYACCCUY, located within 25-nt of the 5′ splice site in three of the Mer1-responsive meiotic transcripts: *AMA1*, *MER2* and *MER3*. Focusing on the *AMA1* intron, they showed that multi-base substitutions within the enhancer element abolished Mer1 splicing activation without affecting the basal level of splicing in vegetative cells not expressing Mer1 (15). Here, we conducted a mutational analysis of the corresponding Mer1 enhancer elements in the *MER3* and *SPO22* introns. First, the invariant central CCC triplets in the putative enhancers of the *MER3* and *SPO22* transcripts were changed to GGG. In both cases, this maneuver abolished Mer1-activated splicing (Figure 4A and B). We then proceeded to conduct a finer analysis of the *SPO22* intronic enhancer, by replacing the conserved cytidines singly with guanosine. The *GCC* and *CGC* variants of *SPO22* were unresponsive to Mer1; their splicing efficiencies in the presence of Mer1 (24% and 26%, respectively) were little better than that of wild-type *SPO22* in the absence of Mer1 (18%) (Figure 4C). The *SPO22-CCG* variant was partially responsive to Mer1, attaining 41% splicing efficiency in Mer1-expressing cells, versus 88% for the wild-type *SPO22* control (Figure 4C).

To better define structure-activity relations in the *SPO22* enhancer, the central cytidines were replaced with uridines, singly and *en masse* (Figure 4D). The *SPO22-UUU* mutant was spliced with 45% splicing efficiency in Mer1-expressing cells, versus 86% for the wild-type *SPO22* control (Figure 4D). The triple C-to-U change was clearly less deleterious than the triple C-to-G mutation (Figure 4B). Virtually all of the impact of the *UUU* mutation could be attributed to the change in the first pyrimidine position, insofar as the *UCC* variant (52% splicing) resembled *UUU*, whereas the single changes as the second and third positions had no apparent effect on the extents of *SPO22* splicing in cells expressing Mer1 (85% and 89% for the *CUC* and *CCU* variants, respectively) (Figure 4D).

Effects of Mer1 mutations

Saccharomyces cerevisiae Mer1 is a 270-aa polypeptide composed of two functional modules: a C-terminal KH domain implicated in RNA binding and an N-terminal domain that interacts with the spliceosome and promotes splicing of target mRNAs (22). The KH domain is an ancient protein fold, widely distributed among taxa, that binds single-stranded RNA or DNA (39). KH domains of the type found in Mer1 consist of a three-stranded antiparallel β sheet plus three α-helices packed against one face of the sheet (Figure 5A, top panel). Fenn *et al*. (40) solved the 1.6 Å crystal structure of a KH domain from the human poly(C)-binding protein PCBP2 in complex with a 7-nt single-stranded DNA oligonucleotide that included the internal pentamer sequence 5′-ACCCT, which is the DNA counterpart of the Mer1 RNA enhancer sequence 5′-ACCCU. Reference to the PCBP2–ssDNA complex shows that recognition of the pyrimidine-rich sequence is achieved, in large part, via direct and water-mediated hydrogen bonding interactions of KH amino acid side chains with the polar edge atoms of the T and C nucleobases (Figure 5A, top panel). The four side chains that engage the bases in PCBP2 emanate from the β2 and β3 strands and the α2 helix. Three of these pyrimidine-binding residues are conserved in yeast Mer1 (as Arg209, Arg214 and Lys222); the fourth residue, an arginine in PCBP2, is replaced by glutamine in the yeast Mer1 and homologous KH domains found in several other fungal proteomes (Figure 5A, bottom panel).

Guided by the PCBP2 structure, we introduced alanine mutations in lieu of Mer1 residues Arg209, Arg214, Lys222 and Gln243 and tested the mutant alleles for

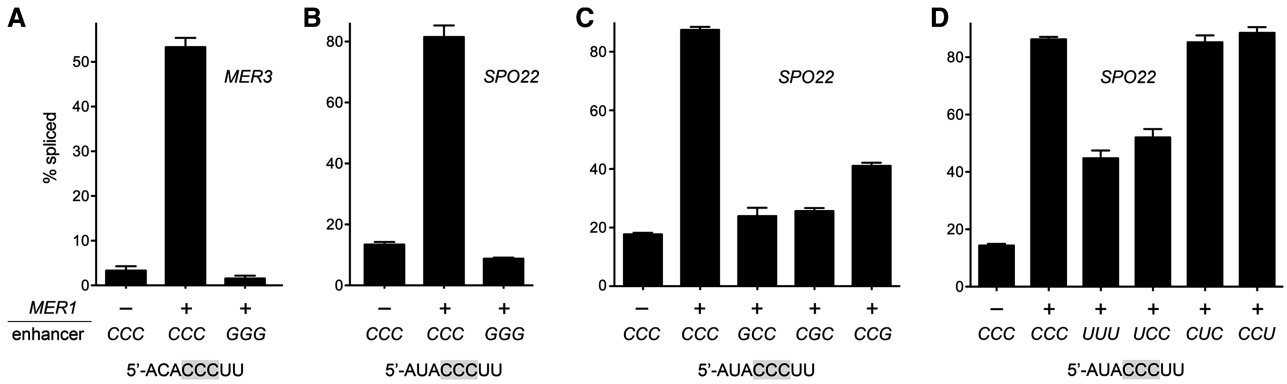

Figure 4. Effects of guanosine and uridine substitutions in the putative Mer1 enhancer elements of the *MER3* and *SPO22* introns. Splicing was gauged by RT–PCR with *MER3* or *SPO22*-specific primers using total RNA template isolated from wild-type haploids that had been transformed with 2 μ *MER3* (**A**), 2 μ *SPO22* (**B–D**), or their intronic enhancer mutant variants as specified plus a 2 μ plasmid for constitutive expression of Mer1 (*MER1*$^{+}$) or an empty 2 μ plasmid control (*MER1*–). The splicing efficiencies are plotted. Each datum is the average of three separate experiments ± SEM.

their ability to activate splicing of *SPO22* pre-mRNAs in vegetative yeast cells (Figure 5B). Whereas *R209A* and *K222A* were as active as wild-type *MER1* in promoting *SPO22* intron removal (82–84% spliced), the *R214A* and *Q243A* mutants were nonfunctional. The 16% *SPO22* splicing seen in *MER1-R214A* and *MER1-Q234A* cells was little better than the 13% *SPO22* splicing in yeast cells that did not express Mer1 (Figure 5B, top panel). Structure-activity relations in the Mer1 KH domain were garnered by introducing conservative substitutions for the essential Arg214 and Gln243 side chains, whereby Arg214 was changed to lysine and glutamine and Gln243 was changed to asparagine, glutamate and arginine (arginine being the native residue at the equivalent position in PCBP2). We found that whereas the *R214K* change revived *SPO22* splicing activity to the level of wild-type *MER1*, the *R214Q* mutant was no better than *R214A* (Figure 5B, bottom panel). We surmise that a positively charged side chain at position 214 of the KH domain is necessary for Mer1 activity. The *Q243E* change elicited a significant, though incomplete recovery of Mer1 function (to 69% *SPO22* splicing versus 87% for wild-type *MER1*) that contrasted with the *Q243N* and *Q243R* mutations (22% and 16% *SPO22* splicing respectively, which were similar to the 18% splicing efficiency in control cells that did not express Mer1) (Figure 5B, bottom panel). We conclude that: (i) a critical distance is required from the protein main chain to the Gln243 amide (i.e. the shorter Asn residue does not suffice); (ii) the putative RNA contacts made by Gln243 differ from those made by the corresponding arginine in the human PCBP2–DNA complex, insofar as a basic arginine side chain was inactive in Mer1, though an acidic glutamate residue functioned almost as well as the native glutamine.

The *MER1* mutants were also surveyed for their activity in promoting the splicing of a different meiotic mRNA target—*MER2* (Figure 5C). The results agreed with the findings for *SPO22*, to wit: (i) Arg209 and Lys222 were not important for *MER2* splicing, but Arg214 and Gln243 were essential; and (ii) *R214K* and *Q243E* restored activity in *MER2* splicing, though the other conservative changes did not.

Determinants of the Nam8-dependence of *PCH2* splicing

Unlike the Mer1-regulated Nam8-dependent transcripts, the *PCH2* pre-mRNA has a perfect consensus 5′ splice site and lacks a Mer1 intronic enhancer sequence. Rather, the *PCH2* transcript is distinguished by its exceptionally long 5′ exonic open reading frame (1551-nt) and a non-consensus intron branchpoint sequence, 5′-CACUAAC (Figure 6). We probed the *PCH2* splicing determinants by: (i) installing a consensus branchpoint sequence in an otherwise native *PCH2* gene; (ii) deleting most of the long upstream exon (while installing a new in-frame AUG codon) to create a *PCH2-Δ5′* variant with a 51-nt 5′ exon; and (iii) combining the *BP* and *Δ5′exon* changes. We tested the *PCH2* mutants on 2 μ plasmids for their splicing efficiency in *NAM8* and *nam8*Δ yeast cells. The results implicate the non-consensus branchpoint and long 5′ exon as separate negative influences on *PCH2* splicing in wild-type cells. For example, shortening the 5′ exon *per se* increased splicing efficiency to 89% for *PCH2-Δexon* versus 70% for the *PCH2* transcript (Figure 6). The consensus branchpoint change *per se* increased splicing efficiency to 91% for *PCH2-BP* (Figure 6). There was no apparent effect of combining the *BP* and *Δexon* changes in wild-type cells. The *PCH2* transcript was spliced with 22% efficiency in *nam8Δ* cells, a 3-fold decrement compared to wild-type cells. The *PCH2-Δexon* transcript was spliced at 83% efficiency in *nam8*Δ cells, signifying that shortening the 5′ exon sufficed to override the Nam8 requirement. The *PCH2-BP* transcript was spliced with 63% efficiency in *nam8Δ* cells, implying that the nonconsensus branchpoint is an independent determinant of Nam8-dependence of *PCH2* splicing, albeit perhaps not as strong a factor as 5′ exon length. Combining the BP and exon changes elicited a further gain of splicing in *nam8Δ* cells to 92% (Figure 6).

Nam8 is a stable component of the U1 snRNP and can be crosslinked to intronic RNA flanking the 5′ splice site (16–18), though the sites of RNA contact within Nam8

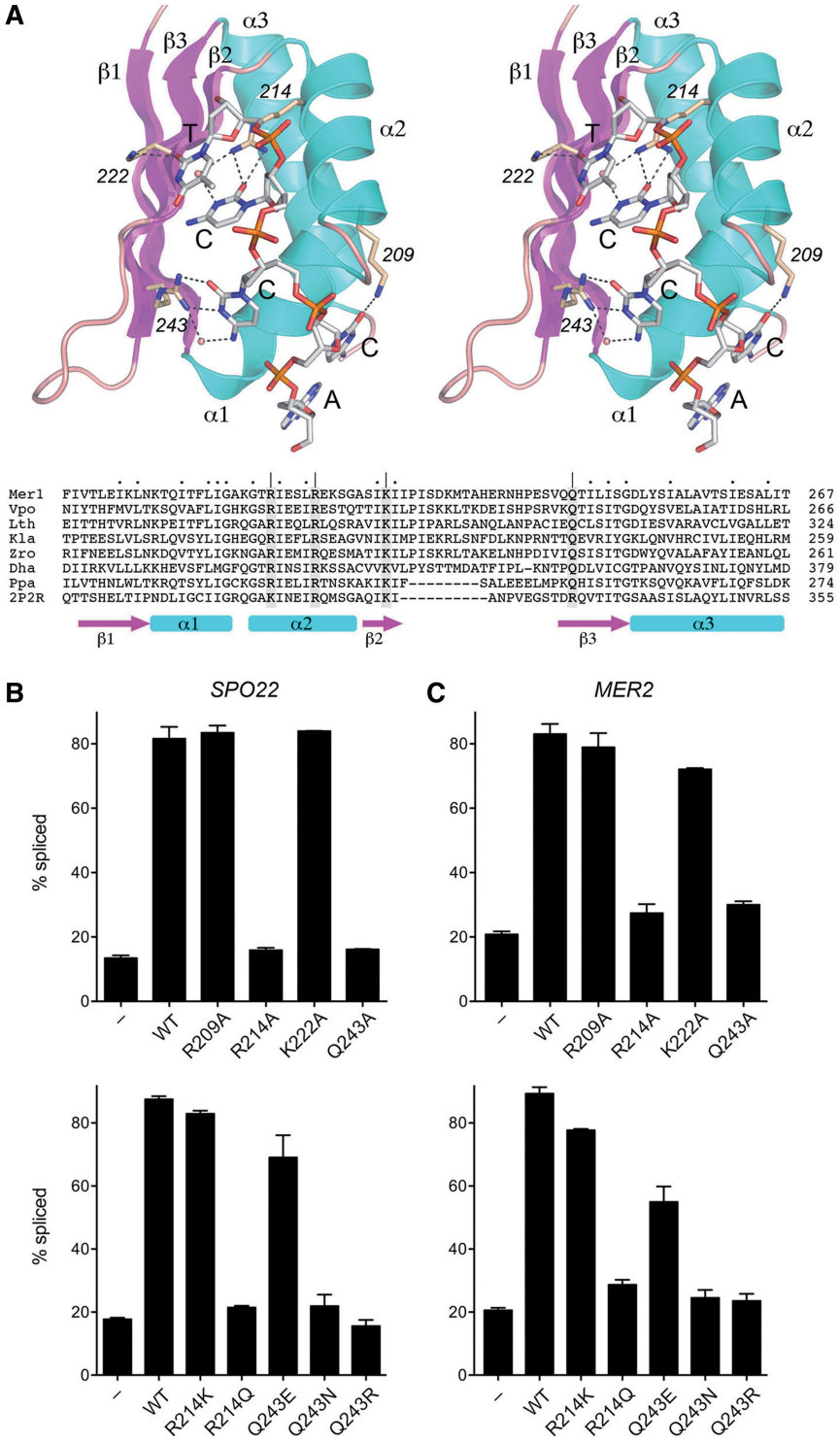

Figure 5. Structure-guided mutational analysis of the Mer1 KH domain. (**A**) (Top) Stereo view of the crystal structure of the KH domain of human PCBP2 bound to a single-stranded DNA oligonucleotide, 5′-ACCCT (pdb id: 2P2R). Side chain hydrogen bonds to the nucleobases are denoted by dashed lines. Waters are rendered as red spheres. The amino acid numbering refers to the equivalent position in the KH domain of yeast Mer1. (Bottom) The primary structure of the *S. cerevisiae* Mer1 KH domain is aligned to homologous KH domains in the proteomes of other fungal taxa—*Vanderwaltozyma polyspora* (Vpo), *Lachancea thermotolerans* (Lth), *Kluyveromyces lactis* (Kla), *Zygosaccharomyces rouxii* (Zro), *Debaryomyces hansenii* (Dha), and *Pichia pastoris* (Ppa)—and to the PCBP2 KH domain. The PCBP2 secondary structure elements are depicted below the amino acid sequence. The RNA-binding side chains of PCBP2 and their counterparts in the fungal KH domains are highlighted in gray boxes; the Mer1 residues subjected to mutational analysis are denoted by vertical line. Other positions of side chain identity/similarity in all eight proteins are indicated by dot above the alignment. (**B**) Effects of Mer1 KH domain mutations on *SPO22* and *MER2* splicing. Splicing was gauged by RT–PCR with *MER2* or *SPO22*-specific primers using total RNA template isolated from wild-type haploids that had been transformed with 2 μ *SPO22* plus a 2 μ plasmid for constitutive expression of wild-type Mer1 or the indicated Mer1 missense mutants, or with an empty 2 μ plasmid control (−). The splicing efficiencies are plotted. Each datum is the average of three separate experiments ± SEM.

have not been mapped. Nam8 contains three tandem RRM (RNA recognition motif) domains that are candidates to mediate the imputed intron RNA-binding function of Nam8. The mammalian TIA-1 protein—also a triple RRM-containing polypeptide and a putative homolog of yeast Nam8—has been shown to regulate pre-mRNA splicing by binding to U-rich sequences flanking the 5′ splice site (19). Thus, it is noteworthy that the *PCH2* intron contains two U-rich polypyrimidine tracts: an 11-mer element (5′-UUUUUUCUUU) immediately adjacent to the 5′ splice site, and a 24-mer element (5′-UUCUUUUUCUUUCUUUCCUUCUUC) located between the 5′ splice site and the branchpoint (Figures 6 and S1). We considered that one or both of these *PCH2* polypyrimidine tracts might act as Nam8 enhancers (akin to the Mer1 enhancer discussed above) and thereby be important for the observed Nam8-dependence of *PCH2* splicing. To test this idea, we deleted the proximal or distal U-rich tracts *en bloc* from an otherwise wild-type *PCH2* transcript (retaining the long 5′ exon and deviant branchpoint) and assayed splicing efficiency of these mutants pre-mRNAs (named *UΔ1* and *UΔ2* respectively) in *NAM8* and *nam8Δ* yeast (Supplementary Figure S1). Splicing of the *UΔ1* transcript in *NAM8* cells (72%) was similar to that of the wild-type *PCH2* RNA (69%). Deleting the distal polypyrimidine tract in *UΔ2* had a mild effect of splicing efficiency (56% in *NAM8* cells) but did not alleviate Nam8 dependence, i.e. 18% of the *UΔ2* transcript was spliced in *nam8*Δ cells (Supplementary Figure S1). Splicing of mutant transcript *UΔ1*+*UΔ2*, in which both U-tracts were deleted, was similar to the *UΔ2* single-deletant (Supplementary Figure S1). These results exclude the idea that Nam8 promotes *PCH2* splicing via obligate specific interactions with one or both of the U-rich polypyrimidine element of the *PCH2* intron.

The *PCH2* intron is a portable determinant of Nam8 dependence

We inserted the 113-nt *PCH2* intron within the otherwise intron-less chromosomal yeast *HIS3* gene of *NAM8* and *nam8*Δ haploid yeast cells. The *PCH2* intron was initially placed near the 3′ end of the *HIS3* ORF (after nucleotide +430) to reflect its distal position in the native *PCH2* pre-mRNA (Figure 7A). *HIS3* provides a convenient reporter for gene expression, manifest as histidine prototrophy. The native *HIS3* gene is functional in *NAM8* and *nam8*Δ strains, both of which grow on agar medium lacking histidine (Figure 7B). By contrast, the *HIS3-[PCH2]* gene containing the distally inserted *PCH2* intron was functional in *NAM8* cells, but not in the *nam8Δ* background (Figure 7B). The salient finding was that a single C-to-U mutation in the intron of the *HIS3-[PCH2]* reporter that restored a consensus branchpoint (Figure 7A) sufficed to restore *HIS3* function in *nam8*Δ cells (Figure 7B). These results show that the *PCH2* intron, by virtue of its deviant branchpoint, is an autonomous determinant of Nam8-dependence in the absence of other *PCH2* gene elements (i.e. promoter, 5′ and 3′ exons, 5′ and 3′ untranslated regions). To evaluate the contributions of 5′ exon length to the Nam8-dependence of *PCH2* intron removal, we repositioned the *PCH2* intron proximally within the *HIS3* reporter (inserting it at nucleotide +48). This maneuver sufficed to allow *nam8*Δ cells to grow in the absence of

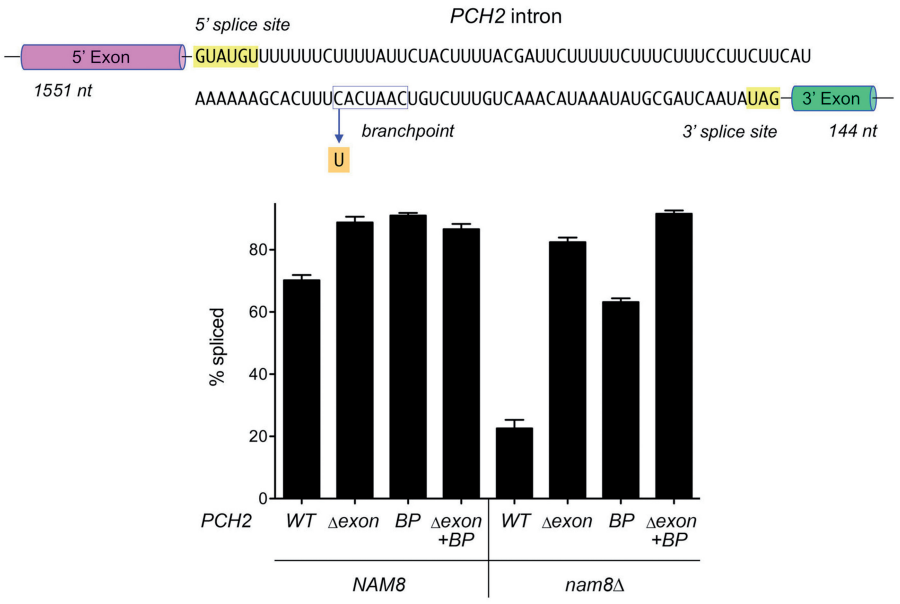

Figure 6. Determinants of the Nam8 dependence of *PCH2* pre-mRNA splicing. The nucleotide sequence of the *PCH2* intron is shown, highlighting its nonconsensus branchpoint and the *BP* mutation that restored a consensus element. The sizes of the flanking protein encoding 5′ and 3′ exons are indicated. The 5′ coding exon in the *Δexon* mutant was shortened to 51 nt. The intronic C-to-U mutation (*BP*) that restored a consensus branchpoint is illustrated. Splicing was gauged by RT–PCR with *PCH2*-specific primers using total RNA template isolated from wild-type (*NAM8*) or *nam8Δ* haploids that had been transformed with 2 μ *PCH2* or its *BP* or *Δexon* mutant variants as specified. The splicing efficiencies are plotted. Each datum is the average of three separate experiments ± SEM.

added histidine (data not shown). These results implicate Nam8 in recognition and/or utilization of the nonconsensus *PCH2* branchpoint in the context of a pre-mRNA substrate with a relatively long 5′ exon.

Domain requirements for Nam8 function

The present findings that Nam8 governs two distinct meiotic splicing pathways prompted us to demarcate the functional domains of Nam8, about which virtually nothing is known, and to gauge whether different Nam8-dependent events rely on different structural features of the Nam8 protein. Nam8 is a 523-aa polypeptide (Figure 8A) that includes three RRM domains (Figure 8B). The closely spaced RRM1-RRM2 tandem unit is preceded by a 40-aa N-terminal leader peptide and separated from the downstream RRM3 domain by a hydrophilic 63-aa inter-RRM linker peptide rich in Ser ($n = 12$), Asn ($n = 11$) and Gln ($n = 8$) (Figure 8A). Distal to RRM3 is a hydrophilic 130-aa C-terminal extension that is also rich in Ser ($n = 17$), Asn ($n = 18$) and Gln ($n = 15$) (Figure 8A). Proteins with primary structure similarity across the entire Nam8 polypeptide can be found in the proteomes of other fungi, including *Neurospora crassa* (491-aa), *Kluyveromyces lactis* (589-aa), *Candida glabrata* (555-aa) and *Ashbya gossypii* (566-aa). Many other fungi encode shorter proteins (~400-aa) that retain the three RRMs, but are missing the Nam8 C-terminal domain. An alignment of the primary structures of *S. cerevisiae* and *A. gossypii* Nam8 (Figure 8A) helped guide the design of serial N and C terminal truncations of *S. cerevisiae* Nam8 at the putative domain (or subdomain) boundaries indicated by the forward and reverse arrowheads in Figure 8A. The truncated open reading frames were cloned into *CEN* plasmids under the control of the native *NAM8* promoter and tested for function *in vivo*.

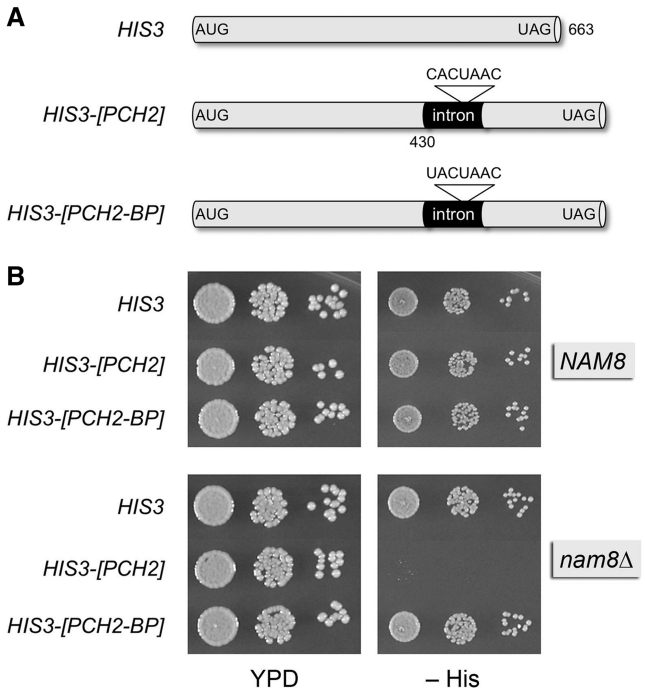

Figure 7. Installation of the *PCH2* intron renders *HIS3* expression Nam8-dependent. (**A**) Schematic depiction of the *HIS3* reporter genes. The *HIS3* ORF is shown in gray; the *PCH2* introns are colored black with the branchpoint sequence in the expanded view. (**B**) Serial dilutions of isogenic *NAM8* and *nam8Δ* cells harboring the indicated chromosomal *HIS3* cassettes were spotted in parallel on to YPD agar medium (left) or synthetic drop-out medium lacking histidine (right). The plates were incubated at 30°C and photographed after 2 days (YPD) or 3 days (–His).

Because deletion of *NAM8* has no apparent impact on yeast growth at 18°C to 37°C, we took advantage of synthetic genetic interactions between *nam8Δ* and deletions of other nonessential yeast genes implicated in pre-mRNA splicing to assay for complementation of growth by the Nam8 truncation mutants. For example, a *nam8Δ tgs1Δ* strain that lacks Nam8 and Tgs1 (a nonessential enzyme that synthesizes the trimethylguanosine cap found on the U1, U2, U4 and U5 snRNAs) is slow growing at 37°C, but inviable at ≤30°C (32). Growth of *nam8Δ tgs1Δ* at 30°C was restored by a *CEN* plasmid encoding full-length Nam8 (aa 1–523), whereas the empty *CEN* vector was ineffective (Figure 8B). Deletion of the N-terminal 40-aa leader peptide preceding RRM1 had no apparent impact on complementation of *nam8Δ tgs1Δ*, nor did truncations at the C-terminus to positions 489 or 454 (Figure 8B). Moreover, simultaneous deletion of aa 1–40 and 455–523 in *NAM8-(41–454)* also did not affect complementation (Figure 8B), signifying that the N and C terminal segments are dispensable. By contrast, the next incremental C-terminal deletions, to positions 400 or 280, ablated *nam8Δ tgs1Δ* complementation (Figure 8B). We conclude that: (i) Nam8-(1–400), which contains all three RRMs, is not sufficient for Nam8 activity in this genetic context and (ii) the Nam8 segment from aa 401–454 flanking RRM3 is essential for Nam8 activity. [Prior information on the C-terminus of Nam8 was limited to the observation that a premature stop codon at amino acid 140 eliminated Nam8 function in a different synthetic lethal complementation assay (16).]

The effects of incremental N-terminal deletions that serially removed the RRMs were also instructive. Deletion of the entire RRM1 domain (in the *151–523* and *151–454* alleles) had little impact on *nam8Δ tgs1Δ* complementation, signifying that RRM2 plus RRM3 sufficed for activity. However, deletions of both RRM1 and RRM2 (in the *251–523* and *251–454* alleles) resulted in diminished complementation activity, as gauged by the smaller size of *NAM8-(251–523) tgs1Δ* colonies *vis à vis* the preceding longer versions of Nam8 (Figure 8B). Whereas further deletions into the inter-RRM linker did not worsen Nam8 function (see *281–523* and *291–523*), complementation was abolished by truncating the N terminus to aa 304 (Figure 8B), which is the predicted proximal margin of the RRM3 domain (Figure 8A). This result implicates the ^{291}MSQFIYPVQQQPS^{303} peptide flanking RRM3 as important for Nam8 function in this genetic assay; it is noteworthy that this peptide sequence at the distal end of the inter-RRM linker is well conserved in *A. gossypii* Nam8 (11/13 positions of amino acid identity), whereas the rest of the linker is not conserved (Figure 8A).

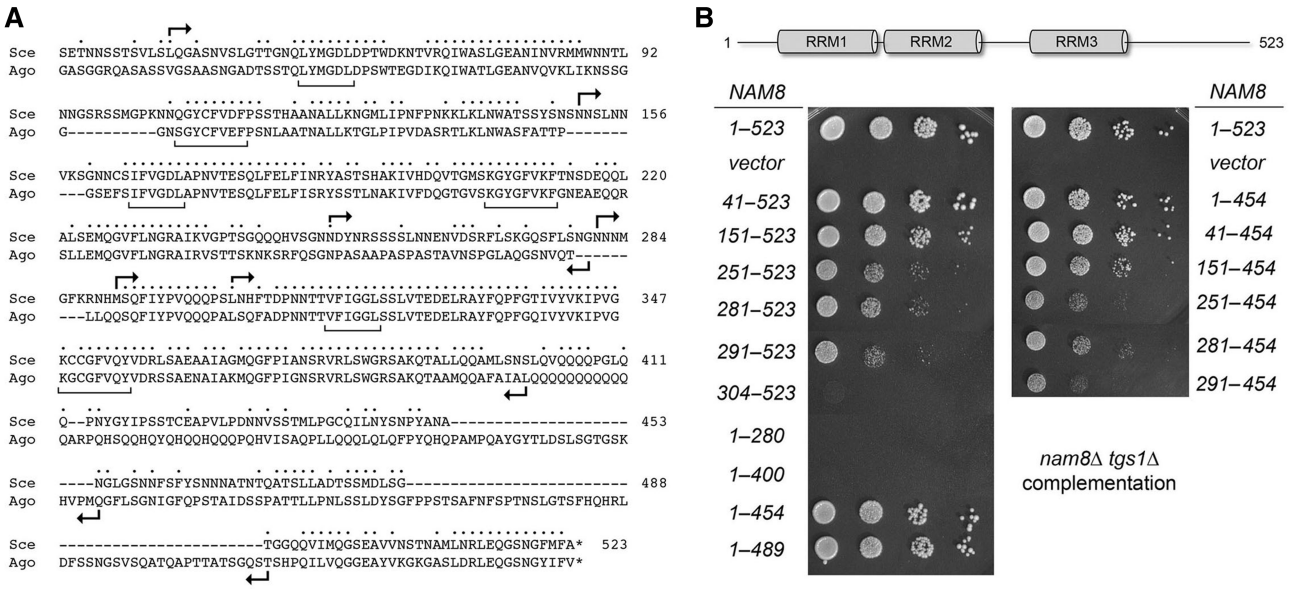

Figure 8. Nam8 domain organization and requirements for complementation of *nam8Δ tgs1Δ*. (**A**) The amino acid sequence of *S. cerevisiae* (Sce) Nam8 from residues 28–523 is aligned to the sequence of *A. gossypii* (Ago) Nam8. Positions of amino acid site chain identity/similarity are denoted by dot above the sequence. RNP2 and RNP1 motifs of the RRMs are indicated by brackets under the sequence. Forward and reverse arrowheads indicate the boundaries of the N and C terminal truncations of Nam8, respectively. (**B**) (Top) Schematic representation of Nam8 domain organization; the RRMs are depicted as cylinders. (Bottom) *CEN LEU2* plasmids bearing wild-type *NAM8* (denoted as *1–523*) or the indicated deletants were tested by plasmid shuffle for *nam8Δ tgs1Δ* complementation. *nam8Δ tgs1Δ* p360-TGS1 (*URA3 CEN TGS1*) cells were transformed with the *CEN LEU2 NAM8* plasmids or the empty *CEN LEU2* vector. Individual Leu^+ transformants were counterselected for growth on FOA agar medium at 37°C. FOA-resistant colonies were patched on SD-Leu agar medium at 37°C. The strains were then grown in liquid culture in SD-Leu medium at 37°C; the cultures were diluted with water to attain an A_{600} of 0.1 and then aliquots (3 μl) of serial 10-fold dilutions (in water) were spotted on YPD agar plates. The plates were photographed after 3 days at 30°C.

To gauge whether the domain requirements for Nam8 function varied with the genetic background in which Nam8 becomes necessary for yeast growth, we performed a parallel series of complementation assays in a *nam8Δ lea1Δ* strain. A synthetic interaction of Nam8 and Lea1 (an inessential stable constituent of the U2 snRNP) was detected in a recent genome-wide genetic array analysis (41). A *lea1Δ* single mutant is temperature--sensitive; it grows well at 20° to 34°C, but very slowly at 37°C (32,42). Here, we constructed a *nam8Δ lea1Δ* double mutant, which was synthetic lethal and required plasmid p360-NAM8 (*CEN URA3 NAM8*) for viability at 30°C (Supplementary Figure S2A). The *nam8Δ lea1Δ* p360-NAM8 strain enabled us to test complementation by plasmid shuffle. Cells transformed with a *CEN LEU2* plasmid bearing full-length *NAM8* plasmid grew on medium containing FOA (a drug that selects against the *URA3* plasmid), while cells transformed with the empty *CEN LEU2* vector (or a vector encoding an inactive Nam8 mutant) did not (Figure S2A). We found that *NAM8* truncation mutants *41–523*, *151–523* and *1–454* permitted growth of 'wild-type' sized colonies on FOA, while the *251–523*, *281–523* and *291–523* alleles yielded small colonies (data not shown). However, cells transformed with mutants *304–523* or *1–400* did not grow on FOA (data not shown). The viable strains were grown in liquid medium and then spot-tested for growth on YPD agar (Figure S2B). Deletion of the N leader peptide plus RRM1 or the C-terminal domain (aa 455–523) had little impact on cell growth *per se*, or in combination (Supplementary Figure S3B). Further N-terminal deletions of RRM2 and parts of the inter-RRM linker resulted in slowed growth, e.g. reflected in smaller colony size of the *291–523* and *251–454* strains (Supplementary Figure S2B). We surmise that the domain requirements for Nam8 function trend similarly in the *lea1Δ* and *tgs1Δ* genetic backgrounds.

The synthetic genetic interactions of Nam8 also embrace Mud1 (41), an inessential component of the U1 snRNP (43). We constructed a *nam8Δ mud1Δ* strain bearing a *CEN URA3 NAM8* plasmid. Although this strain did yield small FOA-resistant colonies under selection at 30°C when transformed with an empty *CEN LEU2* plasmid (data not shown), the vector control cells grew poorly on YPD agar (Supplementary Figure S3). By contrast, transformation with a *CEN LEU2* plasmid expressing full-length *NAM8* resulted in normal-sized FOA-resistant colonies and the cells derived from these colonies grew well on YPD agar (Supplementary Figure S4, *1–523*). The salient findings were that the Nam8 RRM domain requirements for complementation of *nam8Δ mud1Δ* were less stringent than what we observed for *nam8Δ tgs1Δ* and *nam8Δ lea1Δ*. To wit, Nam8-(291–523) and Nam8-(291–454), which lack the leader, RRM1, RRM2 and most of the inter-RRM linker, were as effective as full-length Nam8 in supporting growth in the *mud1Δ* background (Supplementary Figure S3). Moreover, the *304–523* mutant, which was inactive in the *tgs1Δ* and *lea1Δ* strains (Figures 8B and S2), displayed weak complementation activity in *mud1Δ* (Supplementary Figure S3).

A different trend was observed when we tested Nam8 activity in complementation in the synthetic lethal *nam8Δ mud2Δ* background (44). Mud2 is an inessential RRM-containing protein that forms a stable complex with the yeast branchpoint binding protein (BBP) that recruits the U2 snRNP during spliceosome assembly (45,46). We constructed a *nam8Δ mud2Δ* double-mutant, which required either plasmid p360-MUD2 (*CEN URA3 MUD2*) or p360-NAM8 (*CEN URA3 NAM8*) for viability (Figure S4A). Growth of these strains on FOA agar was allowed after transformation with *CEN LEU2* plasmids bearing either *MUD2* or *NAM8*, but not after transformation with the empty *CEN LEU2* vector (Supplementary Figure S4A). We found that *NAM8* N-terminal truncation mutants *41–523*, *151–523*, *251–523* and *281–523* permitted growth of *nam8Δ mud2Δ* cells on FOA, whereas mutants *291–523* and *304–523* did not (data not shown). The viable *NAM8* N-deletants were grown in liquid medium and then spot-tested for growth on YPD agar (Supplementary Figure S4B). These results indicate that the leader, RRM1, and RRM2 are dispensable for Nam8 function in the *mud2*Δ background, though the distal part of the inter-RRM linker is essential. The C-terminal deletant *1–454* supported normal growth in the *mud2*Δ background (Supplementary Figure S4B), but the *1–400* mutant was lethal (no growth on FOA; not shown). Simultaneous deletion of aa 1–40 and 455–523 in *NAM8-(41–454)* did not affect complementation of *nam8Δ mud2Δ* (Supplementary Figure S4B). However, combining the RRM1 deletion with the C-terminal truncation clearly weakened *NAM8-(151–454)* function in the *mud2*Δ background (Supplementary Figure S4B).

Finally, we tested Nam8 function in a different genetic assay predicated on the growth-inhibitory effects of Nam8 overexpression (47). *NAM8* and truncated versions thereof were installed on 2μ *URA3* plasmids under the control of a galactose-inducible promoter. The plasmids were introduced into wild-type cells, which were then tested for growth on –Ura medium containing either glucose (*NAM8* expression repressed) or galactose (*NAM8* expression induced). Whereas all of the strains grew normally on glucose, the galactose-induced expression of full-length Nam8 from the 2μ plasmids inhibited colony formation, an effect not seen with the empty 2μ vector (Supplementary Figure S5). Galactose-dependent growth inhibition was evident for the single N- and C-terminal truncations that scored as active in the synthetic lethal complementation assays: *41–523*, *151–523*, *1–489* and *1–454*, again attesting the dispensability of the leader, RRM1, and C-terminal segment (Supplementary Figure S5). The more extensively truncated versions of *NAM8* that were inactive in the complementation assays (*1–400*, *1–280* and *304–523*) had little or no effect on growth when induced by galactose at high gene dosage. Between these extremes, we saw that N-terminal deletions embracing RRM2 (*251–523* and *281–523*) alleviated the inhibitory effects of galactose induction, albeit not completely (Supplementary Figure S5). The enfeebled dominant negative activity of the RRM2 deletants was consistent with their weakened complementation activity in the *tgs1Δ* and *lea1Δ* backgrounds.

Nam8 domain requirements for splicing of *SPO22* and *PCH2* pre-mRNAs

The full-length and truncated *NAM8* alleles were tested in *nam8*Δ haploids for their activities in Mer1-dependent splicing of the *MER2* pre-mRNA (Figure 9A) and Mer1-independent splicing of *PCH2* pre-mRNA (Figure 9B). *MER2* splicing efficiency was unaffected by loss of the N-terminal leader and C-terminal tail segments, singly or in combination (Figure 9A). Deletion of RRM1 had little impact −66% *MER2* splicing efficiency in *NAM8-(151–523)* cells versus 77% in *NAM8-(41–523)* cells. However, deletion of RRM1 and RRM2 sharply reduced *MER2* splicing efficiency—to 13% in *NAM8-(251–523)* cells, a level barely above the 7% splicing seen in the *nam8Δ* strain (Figure 9A). A C-terminal deletion of the segment from aa 401–454 abolished *MER2* splicing (Figure 9A). Thus, the domain requirements for *MER2* splicing in the presence of Mer1 reflect the trends seen for complementation of *nam8Δ tgs1Δ* (and are apparently more demanding than those for Nam8-dependent vegetative growth in *mud1*Δ and *mud2*Δ backgrounds).

The effects of Nam8 domain deletions on *PCH2* pre-mRNA splicing (Figure 9B) were qualitatively similar to those for *MER2* splicing, although the incremental removal of RRM2 caused a larger reduction in *PCH2* splicing—42% in *NAM8-(151–523)* cells versus 62% in *NAM8-(41–523)* cells and 21% in the *nam8Δ* controls.

Targeted mutations in Nam8 RRM2 and RRM3 guided by the structure of TIA-1

The RRM fold comprises a four-stranded β-sheet flanked on one side by two α-helices, as exemplified in the crystal structure of the RRM2 domain of human TIA-1 (48) (Figure 10A), the putative homolog of the Nam8 RRM2 domain, to which it aligns with 43/80 positions of amino acid identity/similarity (Figure 10B). RRM domains typically bind RNA along the exposed surface of the β-sheet opposite the α-helices (49). The central β1 and β3 strands of the sheet (referred to as the RNP2 and RNP1 motifs, respectively, and denoted by brackets under the Nam8 primary structure in Figure 8A) make most of the atomic contacts with bound RNA.

The present findings that interval deletions of RRM2 plus RRM3 abolished all Nam8 activities prompted us to test the effects of alanine mutations in the putative RNA-binding surfaces of RRM2 and RRM3. The alanine changes were introduced into Nam8-(41–454), a biologically active allele that includes all three tandem RRMs, and the mutants were assayed for complementation of the *nam8Δ tgs1Δ* strain. With respect to RRM2, we tested a single-alanine substitution at Phe166 in the β1 strand RNP2 motif and a triple alanine substitution for Lys205, Tyr207 and Phe209 in the β3 strand RNP1 motif; these side chains project outward on the surface of the β-sheet opposite the two α-helices (Figure 10A) and would correspond to residues in canonical RRMs that interact with RNA. We also combined the RNP2 and RNP1 mutations to generate a quadruple-alanine cluster

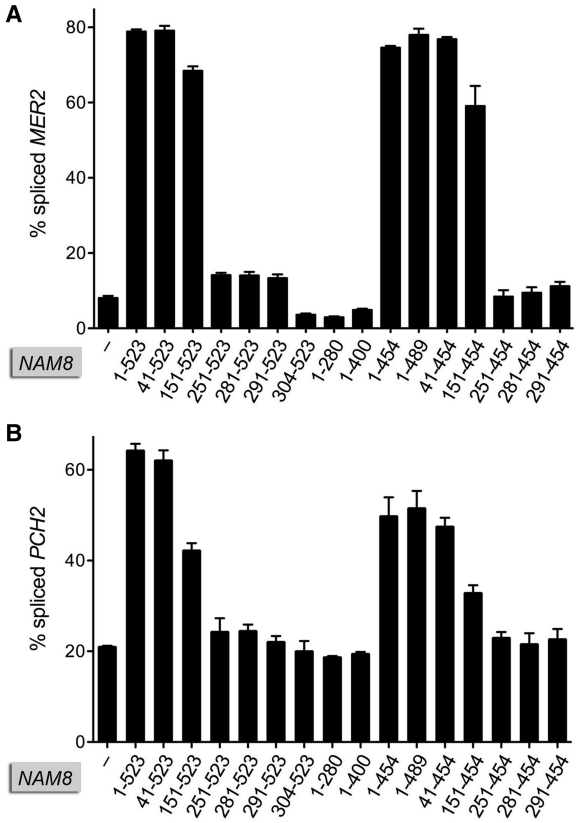

Figure 9. Nam8 domain requirements for splicing of *MER2* and *PCH2* pre-mRNAs. (**A**) Splicing was gauged by RT–PCR with *MER2*-specific primers using total RNA template isolated from *nam8*Δ haploids that had been transformed with the indicated *CEN NAM8* plasmids plus a 2μ plasmid for constitutive expression of wild-type Mer1. (**B**) Splicing was gauged by RT–PCR with *PCH2*-specific primers using total RNA template isolated from *nam8*Δ haploids that had been transformed with the indicated *CEN NAM8* plasmids plus a 2μ *PCH2* plasmid. The splicing efficiencies are plotted. Each datum is the average of three separate experiments ± SEM.

allele, *F166A-K205A-Y207A-F209A*. The *F166A* change *per se* had little effect on Nam8 function in this assay, as gauged by colony size; however, the triple RNP1 mutant and the quadruple mutant resulted in slowed growth and tiny colonies (Figure 10C), similar to the effects of deleting the RRM2 domain on Nam8 function in the *tgs1Δ* background (Figure 8B, *251–454*).

In RRM3, we introduced a single-alanine substitution at Phe316 in the β1 strand and a double-alanine substitution for Lys348, and Phe352 in the β3 strand; also we combined these to make a triple mutant, *F316A-K348A-F352A*. Here, the double RNP1 mutant and the combined RNP2/RNP1 triple mutant were extremely sick (Figure 10C), attesting to a critical contribution of RRM3, and its putative RNA-binding surface, to Nam8 activity when RRMs 1 and 2 are present.

The effects of the RRM mutations on Nam8-dependent splicing of *MER2* pre-mRNA were gauged by transforming *nam8Δ* haploids constitutively expressing Mer1 with *CEN* plasmids bearing the 'wild-type' or alanine-substituted *NAM8-(41–454)* alleles. Subtraction of the side chains at the putative RNA binding surface of the RRM2 and RRM3 domains reduced *MER2* splicing to background levels (Figure 10C).

DISCUSSION

Regulated meiotic splicing in budding yeast is an elegant example of a post-transcriptional 'off–on' switch linked to a developmental program. Whereas only ~5% of yeast genes contain introns, there is an evident enrichment for introns among the genes encoding meiosis-specific proteins, and a tendency for meiotic introns to bear splicing signals that deviate from the norm (31,38). It has been suggested that upregulation of splicing during meiosis—via programmed transition from the splicing 'off' state during vegetative growth—provides added protection against the untimely production of meiotic proteins that could be deleterious to vegetative cells (11,31). Prior studies had characterized a single meiotic splicing regulon controlled by Mer1 and Nam8 and embracing three pre-mRNA targets. The regulatory inputs (if any) to the splicing of the other known meiosis-specific pre-mRNAs are a virtual *tabula rasa* (31). Here, by surveying the full catalogue of meiosis-specific spliced pre-mRNAs for their dependence on Nam8, we've expanded the scope of the Mer1/Nam8 regulon to embrace *SPO22* and illuminated a novel Mer1-independent role for Nam8 in splicing of *PCH2* pre-mRNA. The two flavors of Nam8-dependent splicing differ fundamentally. The Mer1/Nam8-regulated meiotic transcripts share two properties: (i) they have an intronic enhancer sequence, to which Mer1 is thought to bind via its KH domain and (ii) they have non-consensus 5′ splice sites. By contrast, the *PCH2* transcript lacks a Mer1 intronic enhancer and contains a perfect 5′ splice site.

We focused here on dissecting the contributions of the Mer1 enhancer sequence, Mer1 KH domain, and other *SPO22* intronic signals to splicing of *SPO22* pre-mRNA, the newly identified Nam8 target. Whereas *SPO22* has multiple potentially enfeebling non-consensus intronic signals (5′SS, BP and 3′SS), we find that the atypical 5′SS is the decisive factor in Nam8/Mer1 dependence, insofar as a single nucleotide change in the *SPO22* intron that restores a consensus 5′SS overrides the requirements for Mer1 and Nam8. The same scenario applies to the *MER3* intron.

Our studies of *PCH2* splicing implicate the non-consensus 5′-CACUAAC branchpoint and the exceptionally long 5′ exon as separable negative influences on *PCH2* splicing in wild-type cells and as concerted determinants of Nam8-dependence. The finding that Nam8-dependence is portable with the *PCH2* intron, when inserted into the *HIS3* reporter, certifies the importance of the intron and its deviant branchpoint as decisive elements *per se* in the Nam8 requirement. The action of Nam8 in countering a suboptimal *PCH2* branchpoint in the context of a perfect 5′ splice site differs from the case of Mer1/Nam8-dependent splicing, where the intron-bound Mer1 facilitates recruitment of the Nam8-containing U1 snRNP to a suboptimal 5′ splice site

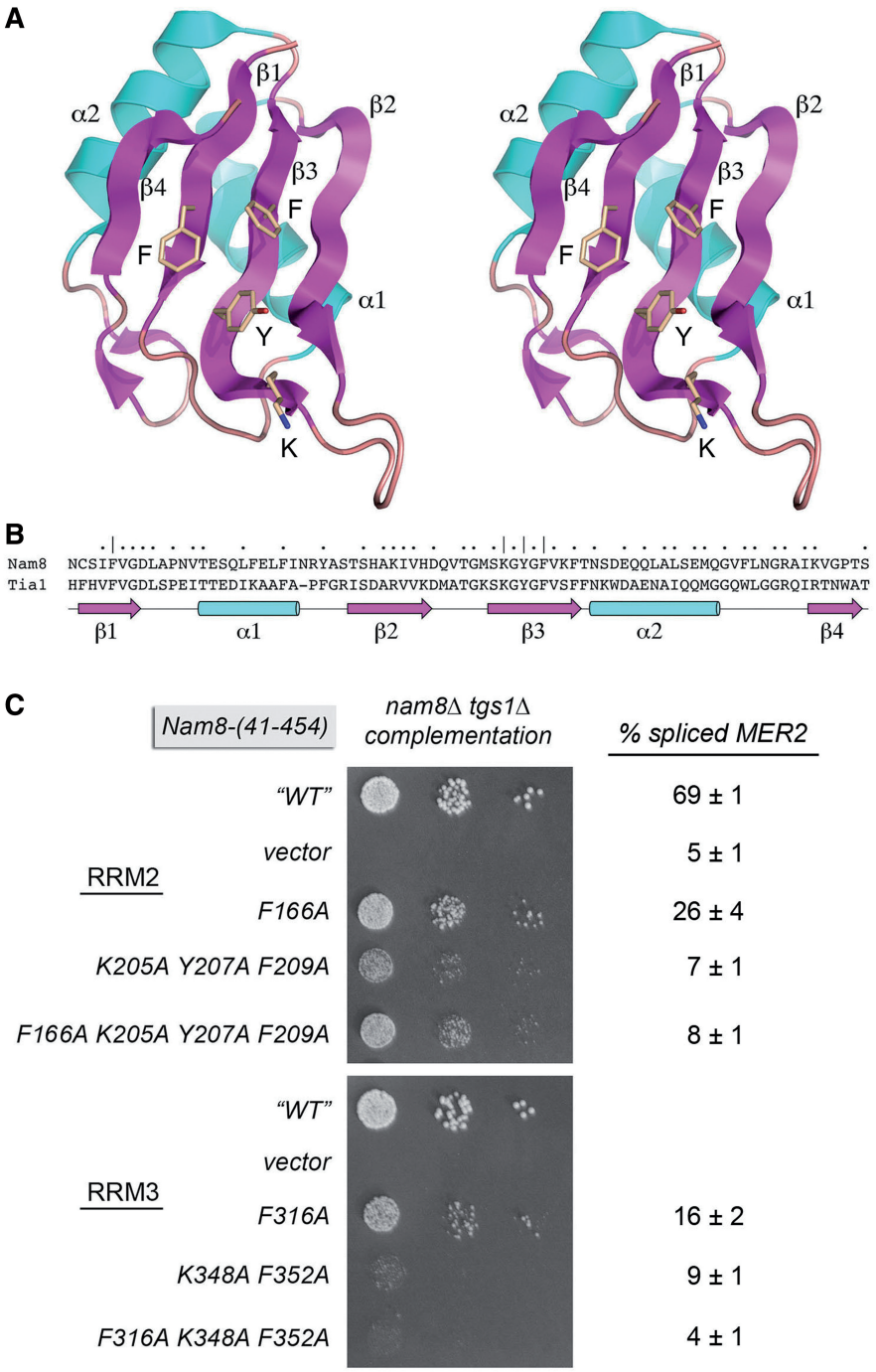

Figure 10. Targeted mutations in the Nam8 RRM domains guided by the structure of TIA-1. (**A**) Stereo view of the crystal structure of the RRM2 domain of TIA-1 (pdb id: 3BS9). The side chains at the putative RNA-binding surface are shown as stick models. (**B**) The amino acid sequences of the Nam8 and TIA-1 RRM2 domains are aligned. The TIA-1 secondary structure elements are depicted below the amino acid sequence. The putative Nam8 RNA-binding residues subjected to mutational analysis are denoted by vertical line. Other positions of side chain identity/similarity are indicated by dot above the alignment. (**C**) The indicated versions of Nam8-(41–454) were tested for complementation of *nam8Δ tgs1Δ* as described in Figure 8. Serial dilutions of liquid cultures were spotted on YPD agar; the plates were photographed after 3 days at 30°C. Mutational effects on splicing were gauged by RT–PCR with *MER2*-specific primers using total RNA template isolated from *nam8*Δ haploids that had been transformed with the indicated *CEN NAM8-(41–454)* plasmids plus a 2μ plasmid for constitutive expression of wild-type Mer1. The splicing efficiencies are shown. Each datum is the average of three separate experiments ± SEM.

(14,15,26) (Figure 11A). Current models invoke bridging contacts between U1 snRNP components Nam8, Snu56 and Snu71 with the enhancer-bound Mer1 in mediating U1 recruitment to the deviant 5′ splice site (22,26) (Figure 11A). We speculate that Nam8 facilitates *PCH2* splicing via macromolecular interactions that recruit the U2 snRNP to the deviant branchpoint (Figure 11B). The participants in this putative interaction network remain to

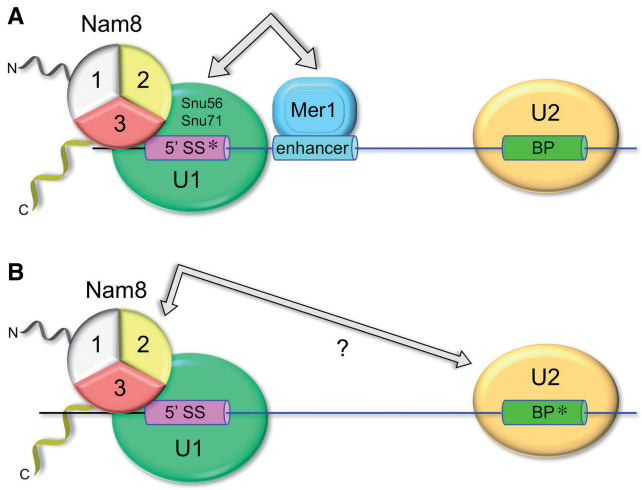

Figure 11. Two modes of Nam8-dependent splicing. (**A**) The Mer1/Nam8 co-dependent splicing regulon embraces four meiotic pre-mRNAs with weak non-consensus 5′ splice sites (5′-SS*). Efficient splicing is achieved when Mer1, bound to an intronic enhancer sequence flanking the 5′-SS*, facilitates recruitment of the Nam8-containing U1 snRNP via proposed Mer1 interactions with U1 proteins Snu56 and Snu71. (**B**) A novel Nam8 splicing regulon, which is independent of Mer1, is defined by the meiotic *PCH2* transcript. The *PCH2* intron has a nonconsensus branchpoint (BP*) that relies on Nam8 for efficient splicing. Because *PCH2* has a consensus 5′-SS, we surmise that Nam8 action in this regulon entails enhanced recruitment of the U2 snRNP to BP*. This step could involve physical interactions (direct or indirect) between Nam8 and the U2 snRNP (or the branchpoint-binding protein Msl5).

be identified. Toward that end, the Nam8-responsive *HIS3-[PCH2]* reporter that we developed here may prove useful in forward genetic screening for yeast mutants that either lose their His prototrophy in *NAM8* cells (as candidate cofactors for Nam8-dependent splicing) or mutants that acquire His prototrophy in *nam8*Δ cells (as candidate suppressors of Nam8-dependency).

The present study illuminates a first set of instructive structure–function relations for the yeast Nam8 protein. As depicted in Figures 8 and 11, Nam8 consists of three RRM domains flanked by N-terminal 'leader' and C-terminal 'trailer' segments. Whereas the distal segment of the trailer domain (aa 455–523) is unnecessary for any Nam8 activity surveyed, our results demonstrate an essential contribution by the proximal part of the Nam8 C-terminal domain (aa 401–454) in all aspects of Nam8 function. One or more of the RRMs are plausible candidates for the imputed intron RNA-binding properties of Nam8. Here, we showed that the N leader and RRM1 are dispensable for Nam8-dependent splicing of meiotic pre-mRNA targets and for Nam8 function in vegetative yeast growth in a variety of synthetic genetic backgrounds. Thus, RRM1 is not implicated in Nam8′s principal contacts to RNA or other components of the splicing apparatus.

Deleting RRM2 along with RRM1 resulted in: (i) disabled Nam8-dependent splicing of *MER2* and *PCH2* pre-mRNAs; (ii) variable effects, ranging from loss of activity to no impact, on Nam8-dependent growth, according to the genetic background being assayed. Because it is possible that RRM1 and RRM2 are functionally redundant, we made an independent test of RRM2 function by targeting alanine substitutions to the putative RNA-binding surface of RRM2 in the context of an otherwise active Nam8 protein that contains all three RRMs. The decrements in vegetative growth in the *tgs1*Δ background and in splicing of *MER2* pre-mRNA implicated RRM2 as a direct participant in Nam8 activity. Nakagawa and Ogawa (21) reported previously that a single mutation, Leu170Pro, in the RNP2 motif (IFVGDL^{170}) of Nam8′s RRM2 domain resulted in a severe defect in meiotic recombination, comparable to that of a *nam8*Δ null. However, we deem this mutational effect as poorly instructive with regard to RRM function, because reference to the equivalent VFVGDL motif in the TIA-1 RRM2 crystal structure (Figure 10B) shows us that the Leu170 side chain is not projecting outward onto the putative RNA-binding surface, but rather points into the hydrophobic core of the RRM (data not shown). Thus, a proline change at this position would be more likely to impact the folding of the RRM2 module than to specifically affect an RNA-binding site.

Extending the N-terminal deletions to the proximal margin of RRM3 (aa 304) abolished or severely weakened all of the Nam8 functions tested. As mentioned above, we attempted to isolate RRM3′s contributions by making alanine changes in the predicted RRM3 RNA-binding surface. The severe defects in vegetative growth in the *tgs1*Δ background and in splicing of *MER2* pre-mRNA caused by the RRM3 alanine clusters implicated RRM3, too, as important for Nam8 activity. Although the results are consistent with an RNA-binding role for either RRM2 or RRM3, it is plausible that one (or both) of the Nam8 RRMs mediates important protein–protein interactions, rather than RNA binding, as has been described for other RRM domains (50).

It is interesting to note that the least demanding genetic function of Nam8 is seen in the *mud1*Δ background, where Nam8-(291–454)—which lacks RRMs 1 and 2—suffices for normal growth. Mud1, like Nam8, is an intrinsic protein component of the yeast U1 snRNP. We presume that the synthetic growth phenotype of the *nam8Δ mud1Δ* double-mutant reflects a gross defect in U1 snRNP structure and function, in which case its full complementation by Nam8-(291–454) implies that this minimized version of Nam8 is assimilated into the U1 snRNP lacking Mud1 and renders it active. That Nam8-(291–454) is not adept at (i) splicing Nam8 meiotic targets with suboptimal introns; (ii) complementing yeast synthetic lethal interactions with splicing factors that are not U1 snRNP components (Lea1, Mud2, Tgs1); or (iii) inhibiting vegetative growth when overexpressed suggests that upstream domains (i.e. RRM2 and the interdomain linker) mediate the invoked interactions of Nam8 with non-U1 splicing factors or the pre-mRNA.

SUPPLEMENTARY DATA

Supplementary Data are available at NAR Online.

ACKNOWLEDGEMENTS

S.S. is an American Cancer Society Research Professor.

FUNDING

U.S. National Institutes of Health grants GM52470 (to S.S.); GM50288 (to B.S.). Funding for open access charges: National Institutes of Health (grants GM52470 and GM50288).

Conflict of interest statement. None declared.

REFERENCES

1. Blencowe,B.J. (2006) Alternative splicing: new insights from global analysis. *Cell*, **126**, 37–47.
2. Nilsen,T.W. and Graveley,B.R. (2010) Expansion of the eukaryotic proteome by alternative splicing. *Nature*, **463**, 457–463.
3. Warf,M.B. and Berglund,J.A. (2010) Role of RNA structure in regulating pre-mRNA splicing. *Trends Biochem. Sci.*, **35**, 169–178.
4. Gabut,M., Chaudry,S. and Blencowe,B.J. (2008) The splicing regulatory machinery. *Cell*, **133**, 192.
5. Biamonte,G. and Caceres,J.F. (2009) Cellular stress and RNA splicing. *Trends Biochem. Sci.*, **34**, 146–1153.
6. House,A.E. and Lynch,K.W. (2008) Regulation of alternative splicing: more than just the ABCs. *J. Biol. Chem.*, **283**, 1217–1221.
7. Tazi,J., Bakour,N. and Stamm,S. (2009) Alternative splicing and disease. *Biochim. Biophys. Acta*, **1792**, 14–26.
8. Fabrizio,P., Dannenberg,J., Dube,P., Kastner,B., Stark,H., Urlaub,H. and Lührmann,R. (2009) The evolutionarily conserved core design of the catalytic activation step of the yeast spliceosome. *Mol. Cell*, **36**, 593–608.
9. Staley,J.P. and Guthrie,C. (1998) Mechanical devices of the spliceosome: motors, clocks, springs, and things. *Cell*, **92**, 315–326.
10. Davis,C.A., Grate,L., Spingola,M. and Ares,M. (2000) Test of intron predictions reveals novel splice sites, alternatively spliced mRNAs and new introns in meiotically regulated genes of yeast. *Nucleic Acids Res.*, **28**, 1700–1706.
11. Maleki,S., Neale,M.J., Arora,C., Henderson,K.A. and Keeney,S. (2007) Interaction between Mei4, Rec114, and other proteins required for meiotic double-strand break formation in *Saccharomyces cerevisiae*. *Chromosoma*, **116**, 471–486.
12. Crotti,L.B. and Horowitz,D.S. (2009) Exon sequence at the splice junctions affect splicing fidelity and alternative splicing. *Proc. Natl Acad. Sci., USA*, **106**, 18954–18959.
13. Engebrecht,J., Voelkel-Meiman,K. and Roeder,G.S. (1991) Meiosis-specific RNA splicing in yeast. *Cell*, **66**, 1257–1268.
14. Nandabalan,K., Price,L. and Roeder,G.S. (1993) Mutations in U1 snRNA bypass the requirement for a cell type-specific RNA splicing factor. *Cell*, **73**, 407–415.
15. Spingola,M. and Ares,M. (2000) A yeast intronic splicing enhancer and Nam8p are required for Mer1p-activated splicing. *Mol. Cell*, **6**, 329–338.
16. Gottschalk,A., Tang,J., Puig,O., Salgado,J., Neubauer,G., Colot,H.V., Mann,M., Séraphin,B., Rosbash,M., Lührmann,R. *et al*. (1998) A comprehensive biochemical and genetic analysis of the yeast U1 snRNP reveals five novel proteins. *RNA*, **4**, 374–393.
17. Puig,O., Gottschalk,A., Fabrizio,P. and Séraphin,B. (1999) Interaction of the U1 snRNP with nonconserved intronic sequences affects 5′ splice site selection. *Genes Dev.*, **13**, 569–580.
18. Zhang,D. and Rosbash,M. (1999) Identification of eight proteins that cross-link to pre-mRNA in the yeast commitment complex. *RNA*, **13**, 581–592.
19. Förch,P., Puig,O., Kedersha,N., Martínez,C., Granneman,S., Séraphin,B., Anderson,P. and Valcárcel,J. (2000) The aopoptosis-promoting factor TIA-1 is a regulator of alternative pre-mRNA splicing. *Mol. Cell*, **6**, 1089–1098.
20. Del Gatto-Konczak,F., Bourgeois,C.F., Le Guiner,C., Hoster,L., Gesnel,M., Stevenin,J. and Breathnach,R. (2000) The RNA-binding protein TIA-1 is a novel mammalian splicing regulator acting through intron sequences adjacent to a 5′ splice site. *Mol. Cell. Biol.*, **20**, 6287–6299.
21. Nakagawa,T. and Ogawa,H. (1997) Involvement of the *MRE2* gene of yeast in formation of meiosis-specific double-strand breaks and crossover recombination through RNA splicing. *Genes Cells*, **2**, 65–79.
22. Spingola,M., Armisen,J. and Ares,M. (2004) Mer1p is a modular splicing factors whose function depends on the conserved U2 snRNP protein Snu17p. *Nucleic Acids Res.*, **32**, 1242–1250.
23. Scherrer,F.W. and Spingola,M. (2006) A subset of Mer1p-dependent introns requires Bud13p for splicing activation and nuclear retention. *RNA*, **12**, 1361–1372.
24. Cooper,K.F., Mallory,M.J., Egeland,D.B., Jarnik,M. and Strich,R. (2000) Ama1p is a meiosis-specific regulator of the anaphase promoting complex/cyclosome in yeast. *Proc. Natl Acad. Sci. USA*, **97**, 14548–14553.
25. Engebrecht,J. and Roeder,G.S. (1990) *MER1*, a yeast gene required for chromosome pairing and genetic recombination is induced in meiosis. *Mol. Cell. Biol.*, **10**, 2379–2389.
26. Balzer,R.J. and Henry,M.F. (2008) Snu56p is required for Mer1p-activates meiotic splicing. *Mol. Cell. Biol.*, **28**, 2497–2508.
27. Nandabalan,K. and Roeder,G.S. (1995) Binding of a cell type-specific RNA splicing factor to its target regulatory sequence. *Mol. Cell. Biol.*, **15**, 1953–1960.
28. Malone,R.E., Pittman,D.L. and Nau,J.J. (1997) Examination of the intron in the meiosis-specific recombination gene *REC114* in *Saccharomyces*. *Mol. Gen. Genet.*, **255**, 410–419.
29. Leu,J.Y. and Roeder,G.S. (1999) Splicing of the meiosis-specific *HOP2* transcript utilizes a unique 5′ splice site. *Mol. Cell. Biol.*, **19**, 7933–7943.
30. Rodriguez-Navarro,S., Igual,J.C. and Perez-Ortin,L.E. (2002) *SRC1*: a intron-containing yeast gene involved in sister chromatid segregation. *Yeast*, **19**, 43–54.
31. Juneau,K., Palm,C., Miranda,M. and Davis,R.W. (2007) High-density yeast-tiling array reveals previously undiscovered introns and extensive regulation of meiotic splicing. *Proc. Natl Acad. Sci., USA*, **104**, 1522–1527.
32. Hausmann,S., Zheng,S., Costanzo,M., Brost,R.L., Garcin,D., Boone,C., Shuman,S. and Schwer,B. (2008) Genetic and biochemical analysis of yeast and human cap trimethylguanosine synthase: functional overlap of TMG caps, snRNP components, pre-mRNA splicing factors, and RNA decay pathways. *J. Biol. Chem.*, **283**, 31706–31718.
33. Chang,J., Schwer,B. and Shuman,S. (2010) Mutational analyses of trimethylguanosine synthase (Tgs1) and Mud2: proteins implicated in pre-mRNA splicing. *RNA*, **16**, 1018–1031.
34. Primig,M., Williams,R.M., Winzeler,E.A., Tevzadze,G.G., Conway,A.R., Hwang,S.Y., Davis,R.W. and Esposito,R.E. (2000) The core meiotic transcriptome in budding yeast. *Nat. Genet.*, **26**, 415–423.
35. Rabitsch,K.P., Toth,A., Galova,M., Schleiffer,A., Schaffner,G., Aigner,E., Rupp,C., Penkner,A.M., Moreno-Borchart,A.C., Primig,M. *et al*. (2001) A screen for genes required for meiosis and spore formation based on whole-genome expression. *Curr. Biol.*, **11**, 1001–1009.
36. Zuker,M. (2003) Mfold web server for nucleic acid folding and hybridization prediction. *Nucleic Acids Res.*, **31**, 3406–3415.
37. Nakagawa,T. and Ogawa,H. (1999) The *Saccharomyces cerevisiae MER3* gene, encoding a novel helicase-like protein, is required for crossover control in meiosis. *EMBO J.*, **18**, 5714–5723.
38. Spingola,M., Grate,L., Haussler,D. and Ares,M. (1999) Genome-wide bioinformatic and molecular analysis of introns in *Saccharomyces cerevisiae*. *RNA*, **5**, 221–234.
39. Valverde,R., Edwards,L. and Regan,L. (2008) Structure and function of KH domains. *FEBS J.*, **275**, 2712–2716.
40. Fenn,S., Du,Z., Lee,J.K., Tjhen,R., Stroud,R.M. and Lames,T.L. (2007) Crystal structure of the third KH domain of human poly(C)-binding protein-2 in complex with a C-rich strand of

human telomeric DNA at 1.6 Å resolution. *Nucleic Acids Res.*, **35**, 2651–2660.
41. Costanzo,M., Baryshnikova,A., Bellay,J., Kim,Y., Spear,E.D., Sevier,C.S., Ding,H., Koh,J.L., Toufighi,K., Mostafavi,S. *et al.* (2010) The genetic landscape of a cell. *Science*, **327**, 425–431.
42. Caspary,F. and Séraphin,B. (1998) The yeast U2A'/U2B'' complex is required for pre-spliceosome formation. *EMBO J.*, **17**, 6348–6358.
43. Liao,X.C., Tang,J. and Rosbash,M. (1993) An enhancer screen identifies a gene that encodes the yeast U1 snRNP A protein: implications for snRNP protein function in pre-mRNA splicing. *Genes Dev.*, **7**, 419–428.
44. Wilmes,G.M., Bergkessel,M., Bandyopadhyay,S., Shales,M., Braberg,H., Cagney,G., Collins,S.R., Whitworth,G.B., Kress,T.L., Weissman,J.S. *et al.* (2008) A genetic interaction map of RNA-processing factors reveals links between Sem1/Dss1-containing complexes and mRNA export and splicing. *Mol. Cell*, **32**, 735–746.
45. Abovich,N., Liao,X.C. and Rosbash,M. (1994) The yeast MUD2 protein: an interaction with PRP11 defines a bridge between commitment complexes and U2 snRNP addition. *Genes Dev.*, **8**, 843–854.
46. Wang,Q., Zhang,L., Lynn,B. and Rymond,B.C. (2008) A BBP-Mud2p heterodimer mediates branchpoint recognition and influences splicing substrate abundance in budding yeast. *Nucleic Acids Res.*, **36**, 2787–2798.
47. Sopko,R., Huang,D., Preston,N., Chua,G., Papp,B., Kafadar,K., Snyder,M., Oliver,S.G., Cyert,M., Hughes,T.R. *et al.* (2006) Mapping pathways and phenotypes by systematic gene overexpression. *Mol. Cell*, **21**, 319–330.
48. Kumar,A.O., Swenson,M.C., Benning,M.M. and Kielkopf,C.L. (2008) Structure of the central RNA recognition motif of human TIA-1 at 1.95 Å resolution. *Biochem. Biophys. Res. Commun.*, **367**, 813–819.
49. Sickmier,E.A., Frato,K.E., Shen,H., Paranawithana,S.R., Green,M.R. and Kielkopf,C.L. (2006) Structural basis for polypyrimidine tract recognition by the essential pre-mRNA splicing factor U2AF65. *Mol. Cell*, **23**, 49–59.
50. Kielkopf,C.L., Lücke,S. and Green,M.R. (2004) U2AF homology motifs: protein recognition in the RRM world. *Genes Dev.*, **18**, 1513–1526.